CHALMERS
UNIVERSITY OF TECHNOLOGY

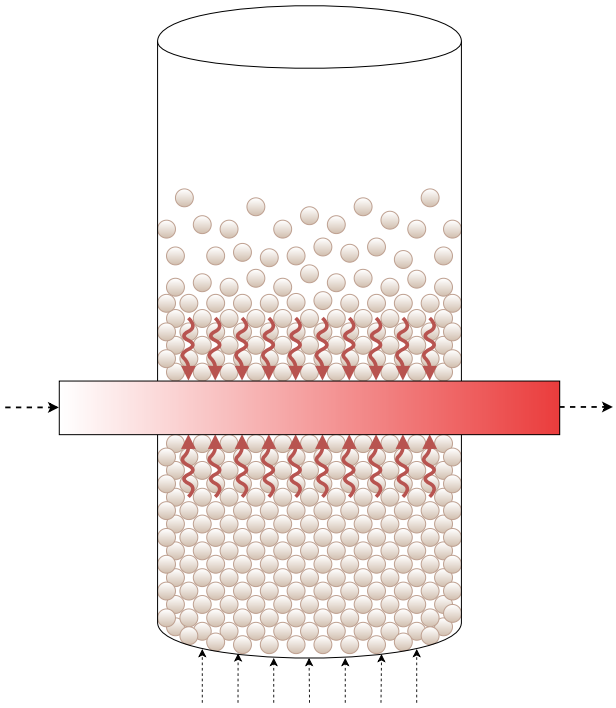

Experimental investigation of the heat transfer coefficient to a horizontal tube submerged in bubbling fluidized bed

Master's thesis in Sustainable Energy Systems

SONJA LÜSCH

Department of Space, Eart and Environment
CHALMERS UNIVERSITY OF TECHNOLOGY
Gothenburg, Sweden 2020

Master's thesis 2020

Experimental investigation of the heat transfer coefficient to a horizontal tube submerged in bubbling fluidized bed

SONJA LÜSCH

CHALMERS
UNIVERSITY OF TECHNOLOGY

Department of Space, Earth and Environment
Division of Energy technology
Chalmers University of Technology
Gothenburg, Sweden 2020

Experimental investigation of the heat transfer coefficient to a horizontal tube submerged in bubbling fluidized bed
SONJA LÜSCH

Supervisor: Viktor Stenberg, Department of Space, Earth and Environment
Examiner: Magnus Rydén, Department of Space, Earth and Environment

Master's Thesis 2020
Department of Space, Earth and Environment
Division of Energy Technology
Chalmers University of Technology
SE-412 96 Gothenburg
Telephone +46 31 772 1000

Cover: Illustration of the bed-to-tube heat transfer in a fluidized bed with a submerged tube

Typeset in LaTeX
Printed by Chalmers Reproservice
Gothenburg, Sweden 2020

Experimental investigation of the heat transfer coefficient to a horizontal tube submerged in bubbling fluidized bed

SONJA LÜSCH
Department of Space, Earth and Environment
Chalmers University of Technology

Abstract

In this thesis, the bed-to-tube heat transfer coefficient has been experimentally investigated in a lab scale fluidized bed to study the effect on varying the bed temperature, bed material, particle size and fluidization gas. Sand and ilmenite are the bed materials evaluated in this work and air, CO_2, steam and flue gas are the tested fluidization gases. These have been tested at temperatures between 400-950 ^oC. The experimental bed-to-tube heat transfer coefficient have been compared to correlations, which are based on heat transfer theory, used for calculating the heat transfer coefficient in fluidized beds.

Today, sand is the most common bed material for combustion of biomass fluidized beds. Ilmenite is of interest because of its oxygen carrier capacity, where it can transport oxygen from an air dense zone to a fuel dense zone in order to improve the fuel conversion and thereby reduce the emissions of CO, unburned hydrocarbons and NO_X. Compared to sand, ilmenite has higher density, which is an interesting parameter to evaluate regarding its influence on the heat transfer. Because of the higher emissivity of the combustion gases CO_2 and steam, radiative heat transfer rate can be higher compared to air, and a higher conductivity can be achieved especially from the steam. Therefore, investigating the effect of how flue gas contributes to the heat transfer rate is also interesting.

The experiments were conducted in a small-scale fluidized bed reactor with a single tube immersed in the bed where water flows. The reactor were located in a furnace which heated up the reactor. The temperature was measured in the bed and in the inlet and exit of the water in the tube. The water flow and the fluidization gas velocity was measured as well. The experiments included investigation of the heat transfer coefficient for ilmenite and sand as bed material at four different particle size range: 90-150, 150-212, 212-250 and 250-355 μm, with the four fluidization gases: air, CO_2, steam and flue gas, at temperatures of 400, 500, 600, 700, 800, and 950 ^oC.

The result showed generally higher heat transfer rate for ilmenite compared to sand, where the smaller particle sizes resulted in a higher heat transfer. The bed that is fluidized by flue gas gave in average a 9.9 % higher heat transfer rate, compared to air as fluidization gas. In this study, the results does not show that CO_2 and steam can contribute to a higher heat transfer rate.

Keywords: heat transfer coefficient, fluidized bed heat exchanger, oxygen carrier, ilmenite

Acknowledgements

First of all, I would like to express my gratefulness to my supervisor, PhD student Viktor Stenberg, for all constructive support and guidance throughout this study. I also want to thank my examiner, associate professor Magnus Rydén, for suggesting the topic and input during the work. PdD student Nasrin Nemati is also acknowledged for the supervision during the experimental part, I am very grateful for the support. Finally, I want to thank research engineers Rustan Hvitt and Johannes Öhlin who always solved all kind of problems that showed up during the experiments.

Sonja Lüsch, Gothenburg, August 2020

Contents

List of Figures

List of Tables

1

Introduction

Since 1750 the CO_2 concentration in the atmosphere has increased with 40%. Greenhouse gas emissions have increased since the pre-industrial era, where the most important drivers are economic and population growth [1]. Around half of the cumulative anthropogenic CO_2 emissions have occurred during the last 40 years and during this time, the CO_2 emissions from fossil fuel combustion have tripled, which results in a contribution of 78% to the total greenhouse gas emission increase.

The increased greenhouse gas emissions have contributed to climate change and increase of global mean surface temperature [1]. With continued emissions of greenhouse gases, the temperature will increase further. To limit the warming and stay below 2 ^{o}C compared to the pre-industrial temperatures, the energy system must be changed to low-carbon energy production. Apart from renewable and nuclear energy, bio-energy with carbon capture and storage can even decrease the atmospheric CO_2 emissions when CO_2 are captured both by the photosynthesis of trees when growing, and during combustion with carbon capture.

1.1 Background

Today's carbon capture technologies and storage are energy demanding and expensive. In conventional methods for CO_2 capture, the separation of CO_2 and N_2 stands for three quarters of the energy required in the process [2]. To avoid this energy intensive step, the CO_2 can be captured already in the combustion reactor by using oxygen carriers. Oxygen carrier consists of a metal oxide, which can replace the bed material in a fluidized bed reactor. Oxygen carriers transport the oxygen from the air to the fuel [3]. By using two reactors, one with air to oxidize the oxygen carrier, and one with fuel which react with the oxidized oxygen carrier, the fuel and air will not be mixed. In the fuel reactor, this chemical-looping process will produce a flue gas stream ideally with only water vapor and carbon dioxide. After condensing of water, the carbon dioxide can be captured in the process and no separation is needed. One promising and inexpensive oxygen carrier to use in both oxygen carrier aided combustion and chemical-looping processes is the iron-titanium mineral ilmenite, $FeTiO_3$ [4].

Fluidized beds are widely used for different purposes such as combustion and gasification. The advantageous characteristics of fluidized bed reactors, such as rapid mixing of solids which leads to almost isothermal conditions, continuous controlled

operations with easy handling of the flow of particles and high rate of heat transfer between the fluidized bed and an immersed object, makes them a preferable choice of reactor [5]. Also the heat and mass transfer rate between gas and solid particles are high in a fluidized bed.

Another promising application for fluidized beds combined with oxygen carrier aided combustion is steam reforming. Compared to conventional methods for steam reforming, the use of fluidized bed as heat source for the steam reforming has the potential to reduce both the fuel consumption and CO_2 emissions [6]. The steam reforming process requires high temperatures at 800-950^{o}C [7]. Because of the high temperatures required, the heat transfer rate is important to consider in order to improve the process efficiency. The bed-to-tube transfer coefficient depends on both convective and radiative heat transfer, which depends on several parameters, for instance the particle size, bed temperature and fluidizing velocity [8]. The particle size is an important factor that influence the heat transfer in a fluidized bed the most [8]. Smaller particles have higher conductive heat transfer between bed and tube surface, since a bed of smaller particles have a smaller gas film thickness and also have shorter residence time on the tube surface.

Previous studies have compared different particle sizes and different bed materials, showed that the heat transfer coefficient increase with decreasing particle size [7], which is consistent with the literature [8]. The study also showed that the choice of bed material influence the heat transfer between the bed material and the tube to different extents [7]. It was shown that ilmenite has promising heat transfer properties compared to sand. The different correlations used in this study consider particle size, density and voidage as important heat transfer properties. The most well-known difference between ilmenite and sand is the larger density of ilmenite, but according to the existing correlations, the density should not affect the heat transfer coefficient as significant as previous studies have shown [7].

The bed-to-tube heat transfer in a bubbling fluidized beds are influenced by both particle convection and gas convection, where the dominant convection type depends on the fluidization gas velocity [9]. At small velocities, from minimum fluidization velocity, the particle convective heat transfer is increasing up to its maximum. Thereafter it will decrease with the gas velocity until its terminal velocity because of the increase in voidage at higher gas velocity. The gas convection is small at low fluidization gas velocities, hence also for small particles. But with larger particle size, the gas convection increases at the same time as the particle convection decreases, and therefore a maximum heat transfer will occur.

The effect on heat transfer have recently been studied by further investigation of the influence of different bed materials but also different fluidization medium [10]. Except air, also recirculated flue gas and steam were studied as fluidization gas, which both contributed to a markedly greater bed-to-tube heat transfer. The bed-to-tube heat transfer increased on average with 45% with steam and 40% with flue gas as fluidization medium for the tested material batches. The combustion gases steam and CO_2 have higher emissivity compared to oxygen and nitrogen, which leads to a higher radiation [11]. In some applications with fluidized bed heat exchanger,

the fluidization gas contains more than just air, for example it can be mixed with recirculated flue gases [10]. This makes a study of its contribution to the bed-to-tube heat transfer of interest. Also because most of the studies of bed-to-tube heat transfer only use air as fluidization medium. The previously mentioned study, was in a larger scale where it is more difficult to control the targeted setpoints and to isolate one parameter at a time, compared to if the test is carried out in a small scale reactor. It was not the same particle size for all the different bed materials that were investigated, which can influence the result, as the particle size is an important factor for the heat transfer. This make a study with more controlled circumstances to be of interest.

The correlations used to calculate the bed-to-tube heat transfer coefficients are determined from experiments at lower temperature, from room temperature up to 400^{o}C, and with usage of sand as bed material [7]. For cases with higher temperatures and other bed materials, it is uncertain if these correlations are reliable when extrapolating from lower temperatures. The idea in this work is to investigate how the choice of bed material influence the bed-to-tube heat transfer coefficient, along with investigation of the influence of the fluidization medium air, flue gas and steam at high temperatures, under controlled circumstances. The results can then be compared with existing correlations to determine if the correlations are accurate at higher temperatures than 400 ^{o}C.

1.2 Aim

The aim of the project is to investigate the bed-to-tube heat transfer coefficient to a horizontal tube submerged in a high temperature bubbling fluidized bed. The project includes an experimental part to investigate the influence of varying the bed material between sand and ilmenite at four different particle sizes. Four different fluidization mediums of air, CO_2, steam and flue gas are tested. The result from the experimental part are then related to existing correlations.

1.3 Limitations

The work is limited to only investigating and comparing sand and ilmenite as bed material, no other bed materials are studied. The fluidization mediums investigated are limited to air, steam, carbon dioxide and a flue gas composition. The influence of the bed-to-tube heat transfer by mixing the fluidization gas with fuel are not investigated. The experiments were taken place in a small scale reactor with an inner diameter of 77.92 mm, and with one tube at the height of 7.5 cm submerged in the bed, during controlled conditions. The influence of adding more tubes to the fluidized bed heat exchanger is not taken into account.

2

Theory

In this chapter, the theory behind fluidized bed and its heat transfer between a tube submerged in the bed, will be presented. Also the theory about using oxygen carrier as bed material for oxygen carrier aided combustion and chemical looping will be presented, as well as introduction to chemical looping for steam reforming in fluidized beds.

2.1 Fluidized beds

In a fluidized bed, the solid bed material particles transforms by fluidization to a fluidlike state through a suspension in gas or liquid [5]. The fluid moves upwards through the bed of fine particles, with a certain velocity. The velocity determines the behaviour of the fluidization. At low velocities, the particles stays stationary which can be seen as a fixed or packed bed [12]. When the velocity increase up to a specific critical value, the bed starts to behave like a liquid. The gas velocity at which this occurs is the minimum fluidization velocity, were the fluid drag is equal to the particles weight less its buoyancy and the bed starts to expand. If the velocity increases further up to another characteristic value, the minimum bubbling velocity, bubbles will rise through the emulsion phase [5], [12]. When increasing the gas velocity in the bubbling fluidized bed, the bed starts to expand and a transition into a turbulent bed will occur. Due to the rapid coalescence and breakup of bubbles in the turbulent bed, the bubble phase will disappear. Heat transfer coefficients in the bubbling bed are higher than those in the turbulent beds, which is because of the higher solid concentration in the bubbling fluidized bed. This thesis will further focus on the bubbling fluidized bed and their characteristics.

2.1.1 Bed material

The bed material for combustion in fluidized beds normally consists of sand. When comparing different bed material, the characteristics of the solid particles depends mostly on its volume and interfacial surface [13]. The ilmenite particles are rarely perfect spherical, and are thereby characterized by their equivalent diameter and their degree of deviation from spherical shape, sphericity. The sphericity can be described through equation 2.1 as the surface area of a sphere with the volume same as the particle divided by the actual area of the particle, where d_v is the volume

diameter, and S is the actual surface area.

$$spehericity(\phi) = \frac{\pi d_v^2}{S} \tag{2.1}$$

The particle size is easiest measured with the sieve size, d_p. The sieve size is the minimum width of a hole in the sieve the particle can pass through. The relation between the sieve size and the volume diameter have been experimentally derived for quartz according to equation 2.2.

$$d_v \approx 1.13 d_p \tag{2.2}$$

In a bed, the particle sizes differ and it is difficult to measure the individual particle sizes. An average particle size is used instead, where the mean particle diameter, $\bar{d_p}$, is calculated through equation 2.3

$$\bar{d_p} = \frac{1}{\sum \left(\frac{x_i}{d_i} \right)} \tag{2.3}$$

where x_i is the weight fraction of samples collected between two adjacent sieves and d_i is the mean aperture diameter of these two sieves.

Another characteristic of the bed material is the voidage, ϵ. The voidage depends on the shape of the particle and their packing characteristics, and can be described by equation 2.4

$$voidage(\epsilon) = \frac{V_v}{V_p + V_v} \tag{2.4}$$

where V_v is the void volume and V_p is the volume of particles.

The minimum fluidization velocity, U_{umf}, is the most important measurement needed for design of fluidized beds [5]. Equation 2.5 is a empirical derived correlation to calculate the minimum fluidization velocity [12].

$$Re_{mf} = \frac{U_{mf} d_p \rho_g}{\mu_g} = \left[C_1^2 + C_2 Ar \right]^{0.5} - C_1 \tag{2.5}$$

where Re is Reynolds number which is expressed in equation 2.6. C_1 and C_2 is empirical constants, which stays almost constant at a Reynolds number between 0.001 and 400 [5]. For fine particles, C_1 and C_2 can be set to 33.7 and 0.0408 respectively [14], according to literature [5]. Ar is Archimedes number, described in equation 2.7

Reynolds number describes the ratio of inertial forces to viscous forces. In equation 2.6, L is the characteristic length, u is the velocity, ρ_g is the gas density and μ_g is the dynamic viscosity of the gas.

$$Re = \frac{L u \rho_g}{\mu_g} \tag{2.6}$$

Archimedes number describes the motion of fluids due to density differences by the ratio of external forces to internal viscous forces. In equation 2.7, g is the acceleration of gravity, ρ_p and ρ_g is the density of the particles and the fluidization gas respectively.

$$Ar = \frac{\rho_g(\rho_p - \rho_g)gd_p^3}{\mu_g^2} \tag{2.7}$$

The minimum fluidization velocity is experimentally derived, and there are several different suggestions on constants for equation 2.5. To ensure the calculated velocity, comparing with other empirical equations to get a reliable result. Another equation for the minimum fluidization velocity can be seen in equation 2.8 [9].

$$Re_{mf} = \frac{U_{mf}d_p\rho_g}{\mu_g} = \frac{Ar}{(1400 + 5.22Ar^{1/2})} \tag{2.8}$$

To avoid carryover of particles from a fluidized bed, the fluidization velocity should be kept between the minimal fluidization velocity and a terminal velocity [5]. The terminal velocity is the velocity when a free falling particle reaches an equilibrium velocity and stops accelerating. This terminal velocity can be described through equation 2.9 [9].

$$Re_t = \frac{U_t d_p\rho_g}{\mu_g} = \frac{Ar}{(18 + 0.61Ar^{1/2})} \tag{2.9}$$

Between the minimal fluidization velocity and the terminal velocity there is a optimum fluidization velocity where the bed-to-tube heat transfer coefficient is at its highest [9]. From minimum fluidization velocity, the particle convective heat transfer is increasing up to its maximum. Thereafter it will decrease with the gas velocity until its terminal velocity, this because of the increase in voidage at higher gas velocity. The gas convection is small at low fluidization gas velocities, hence also for small particles.

$$Re_{opt} = \frac{U_{opt}d_p\rho_g}{\mu_g} = \frac{Ar}{(18 + 5.22Ar^{1/2})} \tag{2.10}$$

2.1.2 High temperature effects

Most of the correlations of minimum fluidization velocity have been done at room temperature, even though most processes in a fluidized bed occurs at a high temperature [15]. Recent studies have shown that the minimum fluidization velocity for both a narrow and wide range of particle size distribution decreased with an increasing temperature, for the temperature range of 300-850 ^{o}C. The decrease of minimum fluidization velocity is likely due to the increasing viscous effect of fluidizing gas on the particles. A simplified correlation for the minimum fluidization velocity, which is consistent even at high temperatures, have been conducted [15], see equation 2.11

$$U_{mf} = \frac{\left(\sum_{i=1}^{n} x_i d_i^{0.55}\right)^{\frac{2}{0.55}} (\rho_s - \rho_g)\, g}{1653 \mu_g} \tag{2.11}$$

High temperature operations also change the behaviour of the fluidized bed [5]. Sintering of particles is one problem that can occur, especially with industrial metals such as metal ores.

2.1.3 Oxygen carrier

In a fluidized bed for combustion of biomass, the solid bed material normally consists of sand. But in order to improve the fuel conversion or separate air from the carbon dioxide formed in reactions with fuel, an oxygen carrier as bed material can be introduced. The oxygen carrier consists of a metal oxide, which transport the oxygen from the air to the fuel [3].

There are criteria for the oxygen carrier to be used in a fluidized bed reactor in order to only produce CO_2 and H_2O and no other diluting gas species. The most important requirement are high reactivity with both fuel and oxygen [16]. Other important criteria are low fragmentation and attrition, low cost, low risk for health and safety, and sufficient oxygen transfer capacity [17].

2.1.3.1 Chemical-looping

In the chemical-looping combustion process, the air will oxidize the oxygen carrier in the air reactor, according to the chemical reaction R 2.1 below, where $MeO_{\alpha-1}$ is used to describe the oxygen carrier in its reduced form while MeO_α is used to express for the oxidized form [16]:

$$MeO_{\alpha-1} + \frac{1}{2} O_2 \leftrightarrow MeO_\alpha \tag{R 2.1}$$

The products from the air reactor is mainly nitrogen gas, N_2, and some oxygen if the air reactor is fed with surplus of oxygen [2]. No formation of thermal nitrogen oxides, NO_x, will occur since the temperature is at a moderate level. In the fuel reactor, the oxidized oxygen carrier will then react with the fuel, which results in only production of water vapour, H_2O, and carbon dioxide, CO_2, which can be seen in the chemical reaction R 2.2 below:

$$C_xH_y + x\, MeO_a \rightarrow x\, CO + \frac{y}{2} H_2 + x\, MeO_{\alpha-1} \tag{R 2.2}$$

Almost pure CO_2 can be collected by condensing the water.

The oxygen carrier will also oxidize CO and H_2 in the fuel reactor, resulting in the chemical reactions R 2.3 and R 2.4 below:

$$CO + MeO_\alpha \leftrightarrow CO_2 + MeO_{\alpha-1} \tag{R 2.3}$$

$$H_2 + MeO_\alpha \leftrightarrow H_2O + MeO_{\alpha-1} \quad \text{(R 2.4)}$$

Fluidized beds are sufficient for chemical looping processes because of the good contact between gas phase and solids, and sufficient solid circulation between the air and fuel reactors [16].

2.1.3.2 Oxygen carrier aided combustion

To improve the fuel conversion in already existing fluidized beds, oxygen carrier as bed material can be introduced for oxygen carrier aided combustion, OCAC, to increase the contact between fuel and oxygen [18]. The oxygen carrier is used to transport oxygen from the oxygen rich part to the oxygen lean zones. In oxygen rich parts of the combustion chamber, the oxygen carrier will be oxidized, such as described in reaction R 2.1. The oxygen carrier will then be reduced in fuel rich parts, which is described in reaction R 2.2. This will lead to reduced emissions of CO and unburned hydrocarbons. Oxygen carrier aided combustion will also reduce the need of excess air since the oxygen is transported by the well mixed bed material to the fuel, which increase the contact between oxygen and fuel. Operating with excess of air is associated with increased heat loss, power consumption and capital cost, due to increased size [18].

2.1.3.3 Ilmenite as oxygen carrier

The oxygen carrier ilmenite, $FeTiO_3$, is a naturally occurring combined oxide [17]. The main application of ilmenite is as feedstock for titanium pigment production [19]. Titanium pigments are used in paints, coatings, plastics. It is also used for titanium metal production and other applications such as pharmaceutical, cosmetics and fibres. Ilmenite naturally occur both as sand and as a rock ore [20]. The main difference between sand ilmenite and rock ilmenite is the shape of the particles, where sand ilmenite have rounded edges and rock ilmenite have more sharp edges. This is because of the naturally weathering, erosion and attrition of the sand ilmenite. Rock ilmenite get its sharp edges from mining och grinding. Ilmenite is well suited as oxygen carrier because of its low-cost material, high reactivity towards syngas and its good fluidization behaviour [17]. The reduced form is $FeTiO_3$ and the oxidized form is $Fe_2TiO_5 + TiO_2$.

Besides the oxygen carrier properties, ilmenite have other promising features as bed material. Ilmenite has, as well as quartz sand, the ability to adsorb with the problematic ash element potassium [21]. But compared to quartz sand, ilmenite does not tend to agglomerate during adsorption. This can give ilmenite increased residence time in a combustion chamber.

2.1.4 Steam reforming in fluidized beds

Chemical-looping technologies are beneficial for reducing CO_2 emissions from large facilities, such as power plants and large industries [22]. But it is more complex to reduce the CO_2 emissions with chemical looping in combustion in smaller facilities, for

example in the transportation sector. One promising option can be to use hydrogen as fuel, which can be produced through steam reforming. Today, the raw material for hydrogen production through steam reforming is mainly natural gas, which is a fossil fuel. In the steam reforming process, the hydrocarbon fuel converts together with steam to synthesis gas, consisting mainly of H_2 and CO, which can be seen in reaction R 2.5. Currently, the hydrogen produced is used for industrial applications, such as fertilizer production, refining industry, metallurgy, for hydrogenation of fats and in manufacturing of high-quality electronic components [2].

$$CH_4 + H_2O \rightarrow CO + 3\,H_2 \tag{R 2.5}$$

Steam reforming in the combination with chemical-looping combustion is a process where steam and hydrocarbons reacts to syngas by conventional catalytic reforming [22]. The chemical-looping combustion system is both capturing CO_2 and providing the endothermic reforming reactions with heat. The temperature in the reformer tubes is in the interval of 700-950 ^{o}C [2]. The reformer tubes can be located inside the fuel reactor in a fluidized bed heat exchanger, which is connected to the chemical-looping system. [22].

2.2 Heat transfer

Heat can be transferred through mainly three different ways, by convective, conductive and radiative heat transfer. These three different type of heat transfer will be explained below.

2.2.1 Convective heat transfer

Convective heat transfer describes the energy exchange between a surface and an adjacent fluid [23]. The rate of convective heat transfer is expressed in equation 2.12

$$q_{conv} = \frac{h_{conv}}{A}\Delta T \tag{2.12}$$

where h_{conv} is the convective heat transfer coefficient. Convective heat transfer can be divided into forced and natural convection [23]. Forced convection is when a external agent, such as fan or pump, make the fluid pass a solid surface and natural convection is driven by the density difference from the temperature variation, which make the fluid circulate next to the solid boundary.

The ratio of the molecular diffusivity of momentoum to the molecular diffusivity of heat can be described through the Prantl number, expressed in equation 2.13

$$Pr = \frac{\mu C_p}{k} \tag{2.13}$$

Equation 2.14 describes the Nusselt number, Nu, which is the ratio of conductive thermal resistance to the convective thermal resistance.

$$Nu = \frac{hd}{k} \tag{2.14}$$

For forced convection, the Nusselt number can be described as a function of Reynolds and Prantl numbers.

2.2.2 Conductive heat transfer

One of the mechanisms behind conductive heat transfer is the molecular interaction where molecules of higher energy gives energy to adjacent molecules at lower energy levels [23]. Conductive heat transfer is present in systems where molecules of a solid, liquid or gas are present and a temperature gradient exist between them. Another mechanism of conduction is heat transferred by free electrons, where the heat transfer depends on the concentration of free electrons. Conductive heat transfer by the free electron mechanism is mainly in pure metallic solids. The conductive heat transfer can be described trough equation 2.15

$$q_{cond} = \frac{kA}{L}\Delta T \tag{2.15}$$

where A is the area normal to the direction of heat flow, L is the depth of the material and k is the materials thermal conductivity.

2.2.3 Radiative heat transfer

Radiative heat transfer differ from convection and conduction in several ways. A medium is not required for radiative heat transfer and the heat transfer depends on both the temperature difference between two bodies and their absolute temperatures [23]. Radiation have both wave properties and particle-like properties and travels at the speed of light. The radiative heat transferred from a surface is given by the Stefan-Boltzman equation 2.16

$$q_{rad} = \sigma T^4 \tag{2.16}$$

where q_{rad} is the radiant heat flux, σ is Stefan-Boltzman constant, which is equal to $5.676 \cdot 10^{-8}$ W/m^2, and T is the surface temperature. The radiative heat transfer coefficient, h_{rad}, can then be described by equation 2.17

$$h_{rad} = \epsilon\sigma(T_b + T_w)(T_b^2 + T_w^2) \tag{2.17}$$

where the emissivity, ϵ, in a fluidized bed, can be can be expressed by equation 2.18 [9].

$$\epsilon = \frac{1}{\frac{1}{\epsilon_b} + \frac{1}{\epsilon_w} - 1} \tag{2.18}$$

ϵ_w is the emissivity of the wall and ϵ_b is the emissivity of the bed, including the emissivity of the combustion gases CO_2 and H_2O [9].

2.2.4 Heat exchangers

The heat transferred in a heat exchanger can be described by equation 2.19

$$Q = U \cdot A \cdot \Delta T_{lm} \tag{2.19}$$

where Q is the heat transfer rate, U is the overall heat transfer coefficient, expressed in equation 2.20, A is the heat transfer area, and ΔT_{lm} is the logarithmic mean temperature difference between the outlet and inlet streams on the outside and the inside of the tube, described in equation 2.21.

In this thesis, a tube heat exchanger immersed in a fluidized bed will be used. Equation 2.20 describes the overall heat transfer for a tube.

$$U = \frac{1}{\frac{1}{h_o} + \frac{d_o \ln(d_o/d_i)}{2k_w} + \frac{d_o}{d_i h_i}} \tag{2.20}$$

The inner and outer heat transfer coefficients are expressed as h_i and h_o respectively, the tube diameter on the inside and on the outside are described as d_i and d_o respectively. k_w is the heat conductivity in the tube wall. The heat transfer through the tube wall depends on the material of the wall.

$$\Delta T_{lm} = \frac{\Delta T_1 - \Delta T_2}{\ln\left(\frac{\Delta T_1}{\Delta T_2}\right)} \tag{2.21}$$

The logarithmic mean temperature difference is described in equation 2.21, where ΔT_1 is the temperature difference between the hot stream entering and cold stream exit the heat exchanger surface. ΔT_2 is the temperature difference between the cold stream entering and hot stream exit the heat exchanger surface.

The heat transfer rate can also be expressed by equation 2.22, where m_i is the mass flow, $C_{p,i}$ is the specific heat capacity and ΔT_i is the temperature difference between the outlet and the inlet of specie i.

$$Q = m_i \cdot C_{p,i} \cdot \Delta T_i \tag{2.22}$$

2.2.4.1 Tube-side heat transfer coefficient

Depending if the fluid inside the tube is laminar or turbulent, different equations are used to calculate the heat transfer coefficient for the tube side [24]. Equation 2.23 is a general equation for turbulent flows

$$Nu = CRe^{0.8}Pr^{0.33}\left(\frac{\mu}{\mu_w}\right)^{0.14} \tag{2.23}$$

where the constant C is 0.023 for non-viscous liquids. For laminar flows, which is when the Reynolds number is below 2000, equation 2.24 can be used [24].

$$Nu = 1.86(RePr)^{0.33}\left(\frac{d_e}{L}\right)^{0.33}\left(\frac{\mu}{\mu_w}\right)^{0.14} \tag{2.24}$$

The heat transfer coefficient can also be correlated from a heat transfer factor, j_h, which can be obtained graphically from figure A.1 in appendix, where it depends

on the Reynolds number and the relation between the length and diameter of the tube. Equation 2.25 can be used to calculate the heat transfer coefficient for both laminar and turbulent flows.

$$h_i = \frac{k_f j_h RePr^{0.33}}{d_i} \left(\frac{\mu}{\mu_w}\right)^{0.14} \tag{2.25}$$

In the tubes, water will be heated by the surrounding tube and bed. A correlation where physical properties of water are conveniently incorporated can be used to calculate the tube-side heat transfer coefficient, which can be seen in equation 2.26

$$h_i = \frac{4200(1.35 + 0.02t)u_t^{0.8}}{d_i^{0.2}} \tag{2.26}$$

where t is the water temperature, u_t is the water velocity and d_i is the inside diameter of the tube.

When the tube wall can be estimated to be isothermal, equation 2.27 can be used to calculate the tub side heat transfer coefficient [25].

$$h_i = \frac{k_{water}\left(\frac{3.657}{\tanh(2.264 \cdot Gz^{-1/3}) + 1.7Gz^{-2/3}} + 0.0499Gz \cdot \tanh\left(Gz^{-1}\right)\right)}{d_i \cdot tanh(2.432Pr_w^{1/6}Gz^{-1/6})} \tag{2.27}$$

where Gz is Graetz number, expressed according to equation 2.28

$$Gz = \frac{Re_D PrD}{x} \tag{2.28}$$

On the shell side of the heat exchanger, there are several factors influencing the heat transfer coefficient in a fluidized bed, which will be described in the next section.

2.2.5 Heat transfer in bubbling fluidized beds

Fluidized beds have a unique ability to rapidly transport heat and maintain a uniform temperature, hence they are used for heat exchange to a large extent in processes where a high heat transfer rate is required [5]. The heat transfer between the bed material and and immersed object is influenced by particle convection or conduction, h_{cond}, gas convection, h_{conv} and radiation, h_{rad}, resulting in the overall gas-side heat transfer coefficient, h_o, which can be seen in equation 2.29 [8]. The radiative heat transfer contributes more to the overall heat transfer coefficient at higher temperatures.

$$h_o = h_{cond} + h_{conv} + h_{rad} \tag{2.29}$$

There are several parameters influencing the bed-to-tube heat transfer coefficient in a fluidized bed, the most dominating parameter has been proven to be the particle size [26]. The heat transfer coefficient increase with an decreasing particle size.

Other parameters that influence the heat transfer coefficient are geometrical factors of the submerged tube bundle, such as distance between tubes and heat transfer tube diameter. Parameters that shows little influence for the hear transfer is the solid particle conductivity and velocity of fluidization gas. Because of difficulty to compute the heat transfer entirely from the theory, mechanistic models, experimental observations and correlations have been developed to describe the heat transfer process [8].

2.2.5.1 Mechanistic model of fluidized beds - The packet renewal model

The packet-renewal model describes the heat transfer by packets of particles in the bulk bed at bed temperature are driven to the heat-transfer surface by the bubbles [8]. While the packet stays in contact with the surface for a short time, τ_p, it cools down, resulting in a reduced temperature difference between the heat-absorbing surface and the heat giving particle. The reduced temperature difference leads to lower heat transfer coefficient. But the packets are all the time replaced by hot particles from the bulk, which leads to high heat-transfer coefficients in a fluidized bed. In the packet-removal model, the heat transfer between the fluidized bed and the heat transfer surface depends on how much of the surface is covered by bubbles. This is because the bubbles contribute to gas convection and the particles contribute both to particle convection and radiation. The heat transfer contribution from the bubble phase is generally less than from the emulsion phase, and are in most cases neglected [8].

2.2.5.2 Experimental observations in fluidized beds

The experimental observations have resulted in operating parameters which are important for the bed-to-tube heat transfer in a bubbling fluidized bed. The most important factor is the particle size, where smaller particles leads to higher heat-transfer coefficients [8]. This, since a bed of smaller particles have a smaller gas film thickness which leads to greater conduction and it also leads to shorter residence time on the tube surface. For very large particles, the gas convection starts to dominate the particle convection. This because the the thickness of the gas layer changes.

Also the fluidization velocity is an important factor for the heat transfer in a fluidized bed. The higher velocity, the shorter residence time on the heat transfer surface, which results in higher heat transfer. But the heat transfer is also influenced by the particle density, which will be reduced at higher fluidization velocities. This leads to a maximum point for the bed-to-tube heat transfer coefficient, where it after a certain fluidization velocity will decrease because of the decreasing concentration of particles at the surface.

2.2.5.3 Heat transfer correlations in bubbling fluidized beds

There are several different empirical correlations for calculating the bed-to-tube heat transfer coefficient in a bubbling fluidized bed. These are described in table 2.1. The common parameters of importance in these correlations is the particle

size, fluidization velocity, density of both bed material and fluidization gas, and also dynamic viscosity and conductivity of the fluidization gas. In order to improve the heat transfer coefficient, changes can be done with respect to the particle size, fluidization velocity and the choice of bed material and fluidization gas with other properties. The properties of the fluidization gas, such as dynamic viscosity and density, are changing with the temperature, thus the bed temperature also influence the heat transfer coefficient.

Table 2.1: Correlations for bed-to-tube heat transfer coefficient

Researchers	**Empirical equation**
Vreedenberg [27]	$\mathrm{Nu} = 420\left[\left(\frac{ud_o\rho_p}{\mu_g}\right)\left(\frac{\mu_g^2}{d_p^3\rho_p^2 g}\right)\right]^{0.3} Pr^{0.3}$
Ainshtein [28]	$\mathrm{Nu} = 5.76(1\text{-}\epsilon)\left(\frac{\rho_g u d_o}{\mu_g \epsilon}\right)^{0.34} Pr^{0.33}(H_b/D_b)^{0.16}(d_o/d_p)$
Gelperin et al. [29]	$\mathrm{Nu} = 4.38\left[\frac{1}{6(1-\epsilon)}\left(\frac{\rho_g u d_p}{\mu_g}\right)\right]^{0.32}\left(\frac{1-\epsilon}{\epsilon}\right)(d_o/d_p)$
Genetti et al. [30]	$\mathrm{Nu} = \frac{11(1-\epsilon)^{0.5}}{\left[1+\frac{0.2512}{\left(\frac{\rho_g u d_p}{\mu_g}\right)^{0.24}\left(\frac{d_p}{0.00203}\right)^2}\right]^2}(d_o/d_p)$
Andeen & Glicksman [31]	$\mathrm{Nu} = 900(1\text{-}\epsilon)\left[\left(\frac{ud_o\rho_p}{\mu_g}\right)\left(\frac{\mu_g^2}{d_p^3\rho_p^2 g}\right)\right]^{0.326} Pr^{0.3}$
Grewal & Saxena [32]	$\mathrm{Nu} = 47(1\text{-}\epsilon)\left(\frac{ud_o\rho_p}{\mu_g}\frac{\mu_g^2}{d_p^3\rho_p^2 g}\right)^{0.325}\left(\frac{\rho_p C_{p,s} d_o^{3/2} g^{1/2}}{k_g}\right)^{0.23} Pr^{0.3}$

The correlations for the bed-to-tube heat transfer is developed at temperatures from room temperature up to 400 ^{o}C. There are uncertainties regarding the validity of the correlations at higher temperatures.

3

Methodology

This chapter describes the procedure of the experimental part with its preparations, experimental set-up, calculations and the final evaluation.

3.1 Theoretical investigation

The correlations for the heat transfer between the fluidized bed and the immersed tube was first used to investigate the theoretically expected heat transfer in the fluidized bed at different bed temperatures. The heat transfer coefficients were calculated for all the different cases that were going to be experimental studied, which is later described in table 3.6. For the theoretically correlations, several parameters varied with the temperature. The parameters that changes with the temperature for the fluidization gas are: density, kinematic viscosity, thermal conduction and the specific heat capacity of the gas. While these parameters change with the bed temperature, the calculated h_o calculated through the correlations in table 2.1 will also change with the bed temperature.

3.2 Preparations

Before the experimental part, preparations with the material and estimations of the running operations was done. Sand and ilmenite were sieved in 4 different particle size ranges, in order to compare how the particle size affects the result but also to be able to compare the two materials at the same particle size. These sieve ranges, as well as the mean particle diameter for the different sieving ranges, can be seen in table 3.1. The sieve ranges was chosen out of the total particle size range of the two materials, and sizes that could be sieved from both materials were chosen. The bed height in the reactor was chosen from the available amount of material, ensuring that the bed totally cover the water tube in the reactor. The fixed bed height were therefore chosen to 13 cm. In order to measure how much of the material were needed to get a fixed bed height of 13 cm, the bulk density was measured by letting the material flow through a funnel into a cylindrical cup with a known volume. The weight of the material was measured, allowing to calculate the bulk density of the material.

Table 3.1: Sieve range of the bed material

Bed material	**Sieve range [μm]**	**Mean particle diameter [μm]**	**Bulk density [g/cm^3]**
Sand X-Small	90-150	120	1,40
Sand Small	150-212	181	1,44
Sand Medium	212-250	231	1,44
Sand Large	250-355	302.5	1,46
Ilmenite X-Small	90-150	120	1,80
Ilmenite Small	150-212	181	1,88
Ilmenite Medium	212-250	231	2,00
Ilmenite Large	250-355	302.5	1,88

The different fluidization gases was chosen to be air, steam and carbon dioxide separately, and a composition of gases oxygen, nitrogen, carbon dioxide and steam that would represent flue gas. The mix and composition of gases in flue gas can be seen in table 3.2.

Table 3.2: Flue gas composition

Compound	$\mathbf{x}_i$
O_2	0.05
N_2	0.59
CO_2	0.15
H_2O	0.21

In order to calculate the bed-to-tube heat transfer coefficient, the tube side heat transfer coefficient must be known. The tube side heat transfer coefficient can be calculated either by equation 2.26 or 2.23 for turbulence fluids, 2.24 for laminar fluids or using equation 2.25 with combination with a graph for the j_h factor. These equations only work when no boiling occur, hence it is of importance to verify no bubbles start to form inside the tube.

The properties of both bed material can be seen in table 3.3. Since not many studies have been done regarding the properties of ilmenite, the emissivity and thermal conductivity was assumed to be the same as for sand. The sphericity was not measured, but studies have shown that the sphericity of rock ilmenite concentrate normally ranging from 0.73 to 0.79, which led to a mean value of 0.76 was used [33].

Bed material	**Heat capacity [J/(kgK)]**	**Sphericity**	**Emissivity**	**Thermal conductivity [W/(mK)]**
Sand	800 [34]	0.80 [13]	0.90 [34]	0.27 [34]
Ilmenite	900 [35]	0.76 [33]	0.90	0.27

Table 3.3: Properties of bed material

3.3 Experimental part

3.3.1 Experimental set-up

The experiments took place in a small-scale fluidized bed reactor, with an horizontal tube submerged in the bed at a height of 75 mm, which can be seen in figure 3.1. The dimensions of the reactor is described in table 3.4. The fluidization medium is fed upwards from a windbox through a distribution plate with 61 holes.

The temperature of the bed was measured by thermocouples at different measurement points which can be seen as number 1-5 in figure 3.1. The measurement points 1-5 have the vertical positions at 3.5, 6.6, 11.6, 16.1 and 31.6 cm respectively in relation to the distribution plate. The measurement takes place close to the reactor wall, located 5 mm into the reactor. The water temperature in the tube were measured with thermocouples before entering the reactor and after exiting the reactor.

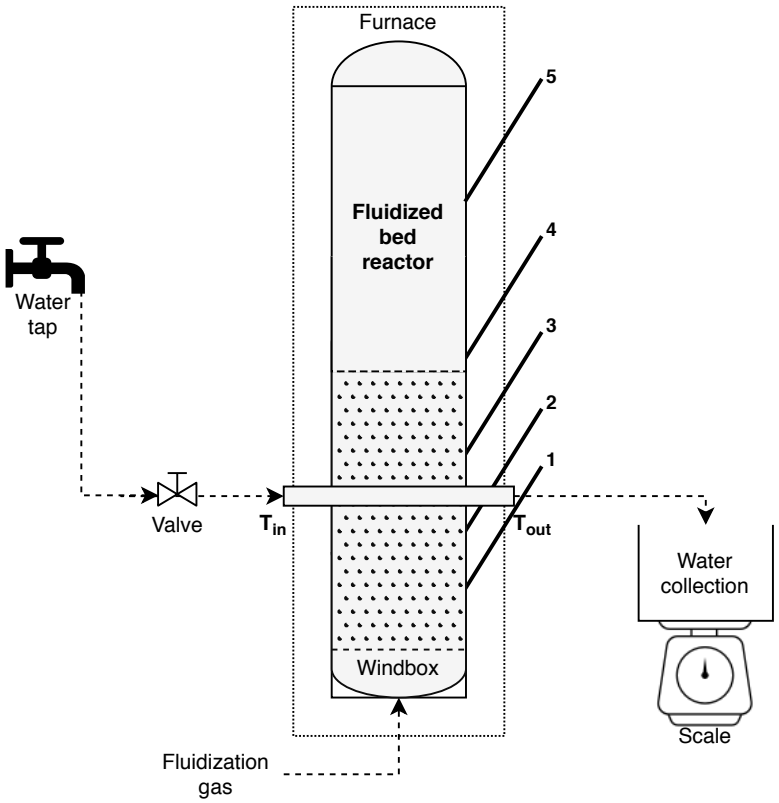

Figure 3.1: Schematic figure of the reactor and the water flow

The controllable parameters were the temperature of the furnace, the flow of fluidization gas and the water flow. The water flow were controlled by a valve and then measured by collecting the outlet water during a specific time and weighted on a scale. The output values from the experiments are water flow, inlet and outlet temperature of the water in the tube and the bed temperature. These values are used to calculate the bed-to-tube heat transfer coefficient from the experimental data.

Table 3.4: Dimensions of reactor

Variable	Value [mm]
Bed diameter, L	77.92
Height of fixed bed, H_{bed}	130
Tube inside diameter, d_i	4
Tube outside diameter, d_o	6
Distribution plate diameter	5
Hole diameter on distribution plate, d_{hole}	0.6

3.3.2 Calculation of h_o from experimental data

First, the logarithmic mean temperature difference was calculated according to equation 2.21 and the heat flux on the tube side through equation 2.22. From this two parameters, the overall heat transfer coefficient, U, can be calculated from equation 2.19. When U is calculated, h_o can be calculated from equation 2.20, where h_i can be calculated from equation 2.26, 2.23, 2.24 or 2.25, depending if the flow is laminar or turbulent. This is decided by calculating Reynolds number using equation 2.6. Either the average of the laminar or the turbulent heat transfer coefficient was then calculated. The bed-to-tube heat transfer coefficient was calculated for different variation of parameters, variation of water flow, variation of fluidization gas velocity and variation of bed temperature.

3.3.3 Determination of water flow

For each bed material at a reference particle size at 212-250 μm and constant bed temperature of 700 ^{o}C and fluidization gas velocity at 0.2 m/s, the water flow in the tube was varied to find a preferable water flow where the bed-to-tube heat transfer coefficient did not change remarkable when increasing the water flow. This means that the water flow is not limiting the heat transfer rate at this point, hence the heat transfer rate is limited on the outside of the tube. This also proved that small changes in water flow during the experiments would not affect the bed-to-tube heat transfer coefficient value significantly.

3.3.4 Determination of fluidization gas velocity

To find a preferable fluidization velocity, the velocity was varied in the interval between 0.025 and 0.3 m/s for each bed material at the particle size range of 212-250 μm, at constant bed temperature of 700 ^{o}C and water flow of 20 ml/s. The preferable fluidization gas velocity was chosen to be one where the bed-to-tube heat transfer coefficient were not changed markedly when changing the fluidization velocity, which means that the gas velocity does not limit the heat transfer rate. The result from varying the fluidization gas velocity was used to decide at which velocity the experiments would be conducted. This will be the total fluidization velocity even for gas mixtures.

3.3.5 Reference case

After evaluating preferable fluidization gas velocity and water flow, a reference case was set with a base value of the parameters that will be varied for both bed material, which can be seen in table 3.5. The parameters were varied one by one while the rest was kept constant, in almost all cases except that the temperature and fluidization gas was varied for all bed material sizes. The reference case was decided to be at a bed temperature of 700 ^{o}C, which is almost in the middle between 400 ^{o}C and 950 ^{o}C, and the reference particle size range was decided to be 212-250 μm, which in the middle between 90 and 355 μm.

Table 3.5: Reference case for comparison

Parameter	**Value**
Fluidization velocity	0.2 m/s
Water flow	20 ml/s
Bed temperature	700 ^{o}C
Particle size range	212-250 μm
Fluidization gas	air

3.3.6 Variation of bed temperature

From the reference case, the bed-to-tube heat transfer coefficient change with the bed temperature for each of the combinations of bed material, particle size and fluidization medium was investigated. The different cases with the combinations of bed material, particle size and fluidization medium can be seen in table 3.6. The heat transfer was measured at the bed temperatures 400, 500, 600, 700, 800 and 950 ^{o}C.

3.4 Evaluation and comparison

To evaluate the result, the bed-to-tube heat transfer coefficient was compared for the different cases, to see if and how it change with changing the different parameters: bed material, particle size, fluidization gas, gas velocity, water flow and temperature.

Table 3.6: Cases with combinations of bed material, particle size and fluidization medium

Case	Bed material	Particle size range [μm]	Fluidization medium
1	Ilmenite	90-150	air
2	Ilmenite	90-150	CO_2
3	Ilmenite	90-150	steam
4	Ilmenite	90-150	flue gas
5	Ilmenite	150-212	air
6	Ilmenite	150-212	CO_2
7	Ilmenite	150-212	steam
8	Ilmenite	150-212	flue gas
9	Ilmenite	212-250	air
10	Ilmenite	212-250	CO_2
11	Ilmenite	212-250	steam
12	Ilmenite	212-250	flue gas
13	Ilmenite	250-355	air
14	Ilmenite	250-355	CO_2
15	Ilmenite	250-355	steam
16	Ilmenite	250-355	flue gas
17	Sand	90-150	air
18	Sand	90-150	CO_2
19	Sand	90-150	steam
20	Sand	90-150	flue gas
21	Sand	150-212	air
22	Sand	150-212	CO_2
23	Sand	150-212	steam
24	Sand	150-212	flue gas
25	Sand	212-250	air
26	Sand	212-250	CO_2
27	Sand	212-250	steam
28	Sand	212-250	flue gas
29	Sand	250-355	air
30	Sand	250-355	CO_2
31	Sand	250-355	steam
32	Sand	250-355	flue gas

4

Results

In this chapter, the result from the different cases will be presented. The different cases will be compared to the reference case in order to determine if the different parameters affect the result.

4.1 Determination of water flow

4.1.1 Ilmenite

When varying the water flow in the case with ilmenite as bed material at a constant bed temperature, and a constant fluidization velocity, the bed-to-tube heat transfer coefficient changed markedly with the water flow at velocities below 18 ml/s, as can be seen in figure 4.1. For water flows above 18 ml/s, the bed-to-tube heat transfer coefficient does not change as much with increasing water flow. Therefore, the water flow to run the experiments with was decided to be 20 ml/s.

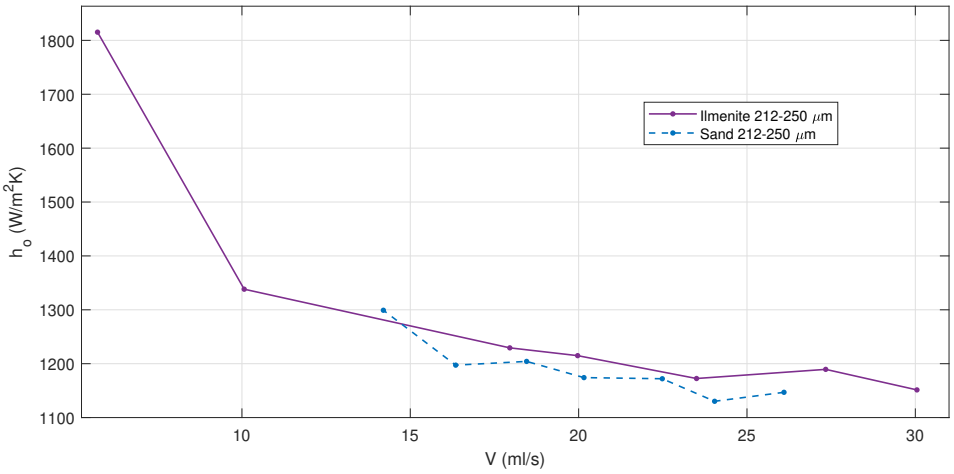

Figure 4.1: Bed-to-tube heat transfer coefficient with variation of water flow with ilmenite as bed material

4.1.2 Sand

As in the case with ilmenite as bed material, when varying the the water flow with sand as bed material, at constant bed temperature, constant fluidization velocity, the bed-to-tube heat transfer coefficient tend to not change markedly with changed water flow at a water flow below 16 ml/s. This can be seen in figure 4.1, and this showed that the experiments could be done with a water flow of 20 ml/s for sand as bed material, as well as for ilmenite.

4.2 Determination of fluidization gas velocity

4.2.1 Ilmenite

For ilmenite as bed material and varying the fluidization velocity at a constant bed temperature and water flow in the tube, the bed-to-tube heat transfer coefficient change greatly at velocities below 0.15 m/s and change less with increasing velocity above 0.15 m/s. This can be seen in figure 4.2. The fluidization velocity to do the experiments with was chosen to be 0.2 m/s.

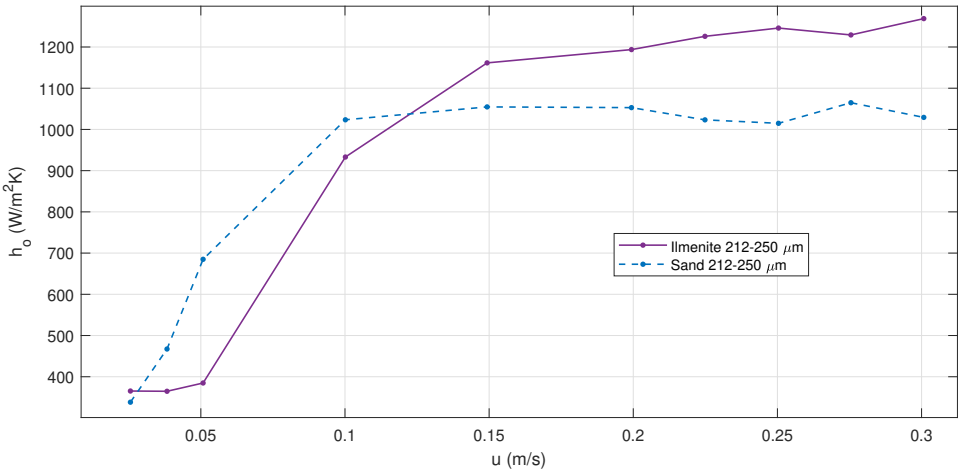

Figure 4.2: Bed-to-tube heat transfer coefficient with variation of fluidization gas velocity with ilmenite as bed material

4.2.2 Sand

When varying the fluidization velocity for the case with sand as bed material, at constant water flow and constant bed temperature, the bed-to-tube heat transfer coefficient tend to act stable at a velocity above 0.1 m/s. Therefore, a fluidization velocity at 0.2 m/s was chosen for the cases with sand as bed material, as well as for the cases with ilmenite.

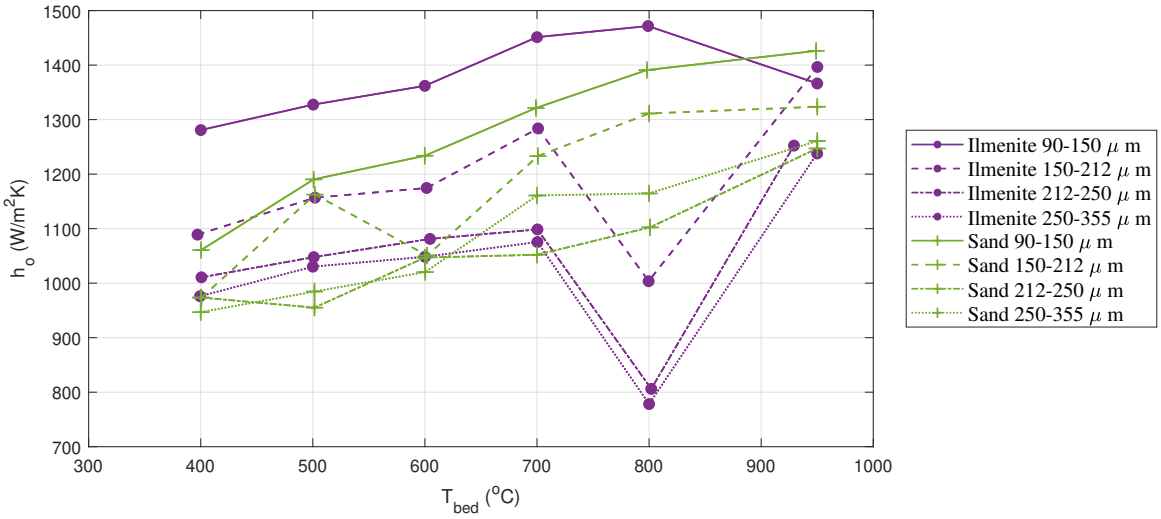

Figure 4.3: Bed-to-tube heat transfer coefficient for the different bed materials ilmenite and sand at different particle size.

4.3 Comparison of bed material

The bed-to-tube heat transfer coefficient for the two different bed material ilmenite and sand is compared in figure 4.3. It can be seen in the figure that ilmenite have generally higher heat transfer coefficient compared to sand of the corresponding particle size range. Except at the bed temperature of 800 ^{o}C where the three largest ilmenite bed materials decrease in heat transfer rate, and then return to reasonable heat transfer rate according to the linear slope before up to 700 ^{o}C. The smallest particle size of ilmenite decrease in heat transfer rate instead at 950 ^{o}C. What could also be seen after the experiments with the smallest particle size of ilmenite, was agglomeration of the particles, which could be a reason to the decrease in heat transfer rate at the highest temperature point. The agglomeration was not harder than it could be mechanically destroyed by hand after operation. The bed-to-tube heat transfer coefficients for sand and ilmenite at the reference temperature of 700 ^{o}C are compared in table 4.1, where the average increase is 2.8 % for ilmenite compared to sand.

Table 4.1: Comparison of the bed-to-tube heat transfer coefficient between sand and ilmenite at the different particle sizes at 700 ^{o}C

Particle size range [μ**m**]	**h$_o$ sand** [**W/m^{2}K**]	**h$_o$ ilmenite** [**W/m^{2}K**]	**Difference** [**%**]
90-150	1321.3	1451.3	+9.8
150-212	1233.1	1283.8	+4.1
212-250	1052.0	1098.6	+4.4
250-355	1160.8	1075.5	-7.4

4.4 Comparison of fluidization medium

The contribution to the bed-to-tube heat transfer by the fluidization medium is compared in graphs for each bed material. In figure 4.4, the different fluidization medium is compared in the bed of ilmenite at a the four different particle size ranges, and in figure 4.5, the fluidization medium are compared when using sand at different particle sizes. The general outcome from these two figures is that flue gas contributes to a higher bed-to-tube heat transfer, with an average increase of 9.9 % compared to air, which can be seen in figure 4.2. The result also shows that CO_2 did not differ significantly from air as fluidization medium regarding the heat transfer. However, it should be noted that the cases with CO_2 contained 43 % CO_2, the rest was air.

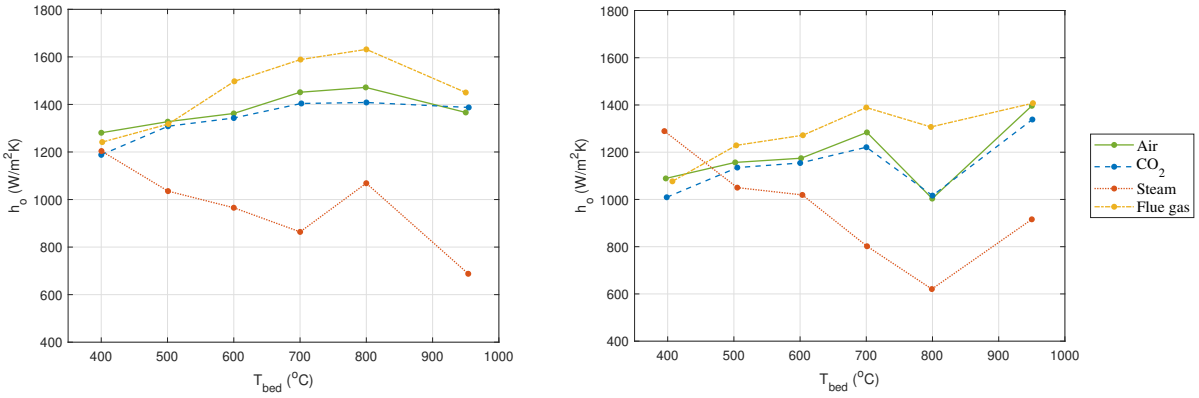

(a) Ilmenite 90-150 μm as bed material **(b)** Ilmenite 150-212 μm as bed material

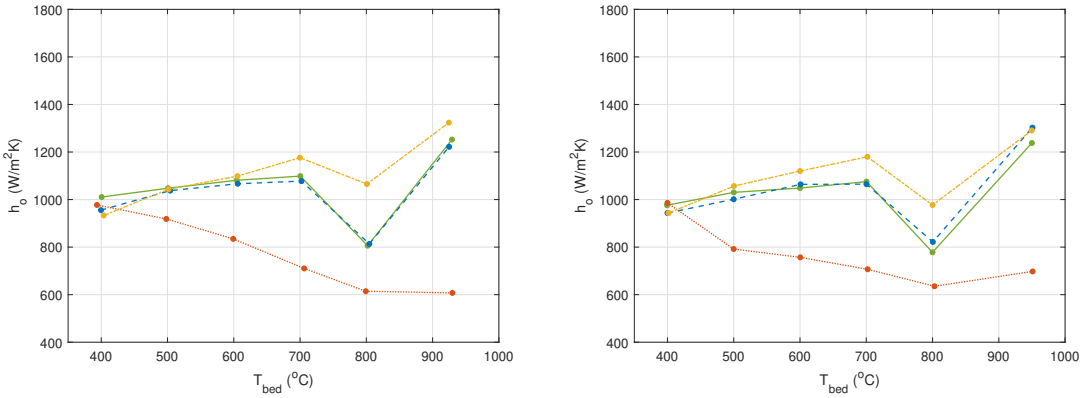

(c) Ilmenite 212-250 μm as bed material **(d)** Ilmenite 250-355 μm as bed material

Figure 4.4: Bed-to-tube heat transfer coefficient for different fluidization medium with ilmenite as bed material

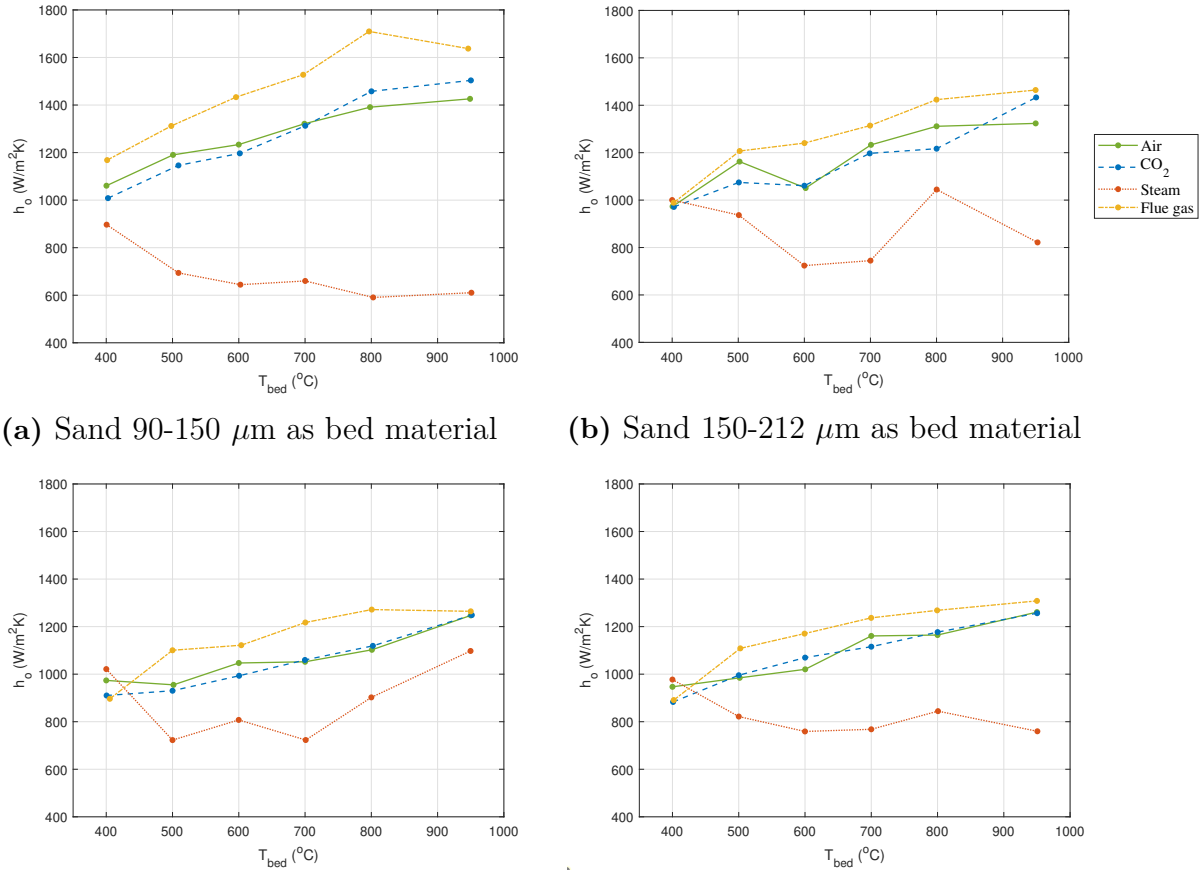

(a) Sand 90-150 μm as bed material

(b) Sand 150-212 μm as bed material

(c) Sand 212-250 μm as bed material

(d) Sand 250-355 μm as bed material

Figure 4.5: Bed-to-tube heat transfer coefficient for different fluidization medium with sand as bed material

Table 4.2: Comparison of the bed-to-tube heat transfer coefficient between the different fluidization medium air, CO_2, steam and flue gas for the different bed materials at 700 ^{o}C, and the percentile difference compared to air

Bed material	particle size [μm]	h_o Air [W/m^{2}K]	h_o CO_2 [W/m^{2}K]	Diff CO_2 [%]	h_o steam [W/m^{2}K]	Diff steam [%]	h_o flue gas [W/m^{2}K]	Diff flue gas [%]
Ilmenite	90-150	1451.3	1404.0	-3.3	863.9	-40.5	1588.8	+9.5
Ilmenite	150-212	1283.8	1221.0	-4.9	801.9	-37.5	1389.1	+8.2
Ilmenite	212-250	1098.6	1077.6	-1.9	710.4	-35.3	1176.2	+7.1
Ilmenite	250-355	1075.5	1064.8	-1.0	706.8	-34.3	1179.9	+9.7
Sand	90-150	1321.3	1312.8	-0.6	660.1	-50.0	1527.4	+15.6
Sand	150-212	1233.1	1197.1	-2.9	744.7	-39.6	1314.3	+6.6
Sand	212-250	1052.0	1059.7	+0.7	723.0	-31.3	1217.4	+15.7
Sand	250-355	1160.8	1115.5	-3.9	768.1	-33.8	1236.8	+6.6

4.4.1 Steam variation in flue gas

The steam generator had a minimum flow of steam. To ensure the same share of steam in the flue gas composition at all temperatures, 43 % of steam was required instead of 21 %. The influence of changing the steam share in the flue gas composition from 21 % to 43 % was investigated at a bed temperature of 400 ^{o}C and is

presented in table 4.3. It can be seen in the table that the bed-to-tube heat transfer coefficient increased with an average of 6.0 % for a steam share of 43 % compared to 21 %.

Table 4.3: Comparison of the bed-to-tube heat transfer coefficient with different amount of steam in the flue gas composition and the percentile change of the heat transfer coefficient from 21% to 43% steam at 400 ^{o}C

Bed material	**particle size** [μ**m**]	**h$_o$ 43% steam** [**W/m^{2}K**]	**h$_o$ 21% steam** [**W/m^{2}K**]	**Difference** [%]
Ilmenite	90-150	1241.6	1238.1	-0.3
Ilmenite	150-212	1076.7	1157.5	7.5
Ilmenite	212-250	933.3	987.6	5.8
Ilmenite	250-355	943.6	997.6	5.7
Sand	90-150	1168.3	1214.1	3.9
Sand	150-212	989.0	1074.5	8.6
Sand	212-250	896.4	914.8	2.1
Sand	250-355	891.0	1018.5	14.3

4.5 Comparison with correlations

The experimentally estimated bed-to-tube heat transfer coefficient compared to the correlations are plotted in appendix A.2 for all the cases. The closest correlation to each of the case can be seen in figure 4.4 together with the percentile root mean square error, RMSE, in relation to the experimental measured value. What can be seen in the table is that the correlation by Grewal & Saxena occurs most times (11 of 32) as the closest correlation followed by the correlation by Genetti (8 of 32). For the fluidization mediums air, CO_2 and flue gas, the correlation by Grewal & Saxena is the most accurate most times (4,3,4 of 8 respectively), while for steam as fluidization medium the closest correlations is the one by Ainshtein (6 of 8).

To consider the influence of the different bed material when comparing with the correlations, the experiments in a bed with ilmenite was most often close to the correlation by Grewal & Saxena (7 of 16). A general trend is also that at small particle sizes of ilmenite (90-212 μm), the correlation by Genetti is often more close to the experimental values while the correlation by Grewal & Saxena is more often close at larger particle size (212-355 μm). For the experiments in a bed of sand particles, the correlations closest to the experimental values were more varied. No trend could be seen regarding correlations accurate at a certain particle size or with different fluidization gases. However, even for the cases with sand as bed material, the correlation by Grewal & Saxena was the one that matched the experimental values best in most cases (4 of 16).

Table 4.4: Most accurate correlation to each of the different cases according to the percentile root mean square error, RMSE

Case	**Closest correlation**	**RMSE** [%]
1 (Ilmenite 90-150μm air) [A.2a]	Grewal & Saxena	38.7
2 (Ilmenite 90-150μm CO_2) [A.2b]	Genetti	36.1
3 (Ilmenite 90-150μm steam) [A.2c]	Andeen & Glicksman	32.6
4 (Ilmenite 90-150μm flue gas) [A.2d]	Genetti	36.9
5 (Ilmenite 150-212μm air) [A.3a]	Genetti	10.8
6 (Ilmenite 150-212μm CO_2) [A.3b]	Genetti	13.9
7 (Ilmenite 150-212μm steam) [A.3c]	Ainshtein	33.1
8 (Ilmenite 150-212μm flue gas) [A.3d]	Genetti	15.2
9 (Ilmenite 212-250μm air) [A.4a]	Grewal & Saxena	25.1
10 (Ilmenite 212-250μm CO_2) [A.4b]	Grewal & Saxena	26.5
11 (Ilmenite 212-250μm steam) [A.4c]	Ainshtein	32.4
12 (Ilmenite 212-250μm flue gas) [A.4d]	Grewal & Saxena	32.7
13 (Ilmenite 250-355μm air) [A.5a]	Grewal & Saxena	17.5
14 (Ilmenite 250-355μm CO_2) [A.5b]	Grewal & Saxena	16.2
15 (Ilmenite 250-355μm steam) [A.5c]	Ainshtein	27.3
16 (Ilmenite 250-355μm flue gas) [A.5d]	Grewal & Saxena	18.5
17 (Sand 90-150μm air) [A.6a]	Andeen & Glicksman	18.3
18 (Sand 90-150μm CO_2) [A.6b]	Andeen & Glicksman	17.9
19 (Sand 90-150μm steam) [A.6c]	Gelperin	35.6
20 (Sand 90-150μm flue gas) [A.6d]	Andeen & Glicksman	9.8
21 (Sand 150-212μm air) [A.7a]	Genetti	8.1
22 (Sand 150-212μm CO_2)[A.7b]	Genetti	11.3
23 (Sand 150-212μm steam) [A.7c]	Ainshtein	22.2
24 (Sand 150-212μm flue gas) [A.7d]	Genetti	15.2
25 (Sand 212-250μm air) [A.8a]	Grewal & Saxena	17.0
26 (Sand 212-250μm CO_2) [A.8b]	Grewal & Saxena	17.7
27 (Sand 212-250μm steam) [A.8c]	Ainshtein	17.4
28 (Sand 212-250μm flue gas) [A.8d]	Grewal & Saxena	27.5
29 (Sand 250-355μm air) [A.9a]	Vreedenberg	6.6
30 (Sand 250-355μm CO_2) [A.9b]	Vreedenberg	6.6
31 (Sand 250-355μm steam) [A.9c]	Ainshtein	21.8
32 (Sand 250-355μm flue gas) [A.9d]	Grewal & Saxena	11.8

5

Discussion

This chapter will discuss the result and what conclusions can be drawn from it together with possible sources of error. The chapter ends with suggestions for future study research.

5.1 Validity of experimental results

The experiments generally got an expected result with h_o in the same range as for the correlations, were the heat transfer changed with the parameters according to the literature. It was however some exceptions from the expected result. The main exceptions was the dip in h_o for the ilmenite bed material at several particle sizes at 800 ^{o}C, and the fluidization by pure steam gave lower heat transfer rate compared to air, which also decreased with increasing temperature. This can be explained by the pulsating flow of steam from the steam generator, which probably resulted in poor fluidization.

One explanation why the heat transfer rate dip at 800 ^{o}C can be because of oxidation of ilmenite which can occur if the material was not fully oxidized before. This could affect the results by reducing the gas flow and changing the gas composition when the oxygen oxidize ilmenite. No reduce of oxygen concentration in the gas stream could however not be seen in the data from the experiments at 800 ^{o}C compared to other temperatures. Apart from this, the experiments gave expected results which agreed with the literature. For the different parameters that were varied, next section will discuss how the parameters influenced the result.

5.1.1 Parameters

Initially investigations of water flow and fluidization gas velocity was done to decide which flow rate the later experiments should be run at. The curve of h_o flattens out, and does not change significantly when increasing the flow rate for both the gas velocity and water flow. This shows that both the water flow and fluidization velocity was set to good values where they would not have a great impact on the experimental result if it would differ during the experiments. This is important for the water flow, which was adjusted with a valve and then weighted during a specific time to determine the water flow. This made it hard to set to exactly the same for all experiments, and hard to decide if it was kept constant during the experiments.

The mainly investigated parameters: bed temperature, particle size, bed material and type of fluidization gas. The type of fluidization gas led to a change in the properties of heat capacity, thermal conductivity, dynamic viscosity and the density of the gas. By changing the bed material, even properties such as particle density, bulk density, emissivity, thermal conductivity, specific heat capacity and sphericity changed. Several of these properties for ilmenite was assumed, including sphericity, emissivity and thermal conductivity. This because there is not many studies done on these properties for ilmenite. These assumed properties were however not verified in this study. This makes the calculations of the correlations with ilmenite as bed material uncertain.

The bed temperature was seen to influence the bed-to-tube heat transfer coefficient by increase it with increasing bed temperature. This was general for both bed material and particle size except a dip for ilmenite at 800 ^{o}C, and almost all fluidization gases except steam, as have been mentioned above.

The particle size was affecting the heat transfer rate by higher heat transfer at small particle sizes and reduced heat transfer when increasing the particle size. This can probably be explained by the larger heat transfer surface per volume of small particles compared to larger particles. One problem with smaller particle size of ilmenite was the agglomeration of the particles, which can be an explanation of the decreased heat transfer rate of the smallest ilmenite particles at the highest temperature, the agglomeration was also confirmed when the reactor was emptied afterwards.

When comparing the different fluidization gases, only flue gas showed to significantly improve the heat transfer coefficient, with an average increase of 9.9 % compared to air when considering all bed materials. Steam did not improve the heat transfer coefficient in this study, which can be explained by the already discussed problem with pulsation and poorly fluidization of the bed. CO_2 could neither be seen to increase the heat transfer coefficient. Reasons for this can be that the bed was only fluidized with 43 % CO_2, the rest was air. This was a result of limitation of the maximum gas flow from the gas bottle. To reach a gas velocity of 0.2 m/s at all temperature steps, air was needed. Since the greater emissivity from CO_2 compared to air only influence the radiative heat transfer, which is a small contribution compared to convective heat transfer, a greater difference would maybe be seen in the fluidization gas if it only contained pure CO_2.

From the investigation of the influence by changing the share of steam in flue gas from the standard of 21 % to 43 %, it was shown that the bed-to-tube heat transfer coefficient increased with 6.0 %. This also shows that the increased h_o by using flue gas as fluidization gas compared to air is probably not as high as 9.9 % in a real case where the share of steam is 21 %. With this in to consideration, an increase of 3.3 % would be more reasonable when comparing the bed-to-tube heat transfer coefficient for flue gas with air as fluidization gas.

5.1.2 Comparison with correlations

None of the correlations could perfectly describe the experimental calculated bed-to-tube heat transfer coefficient, although the correlation by Grewal & Saxena was the one closest to the experimental values in most cases. What also could be seen from the experimental values compared to the correlations, is that the correlation by Genetti is more accurate to the experimental values for small particles and the correlation by Grewal & Saxena was more close to the experimental values at the larger particle sizes. This connection was more clear for the cases with ilmenite as bed material, while the closest correlation to the cases with sand as bed material varied with the four different bed materials. For the smallest, Andeen & Glicksmann were closest, for the second smallest particle sizes, Genetti was closest, Grewal & Saxena was closest to the second largest particle sizes and Vreedenberg was most accurate for the largest particle size.

For the cases where the bed was fluidized with steam, the closest correlation to the experimental values were the correlation by Ainshtein. Since the steam flow was pulsating and not sufficient for a desirable fluidization. Accordingly, the results and closest correlation the cases with steam as fluidization medium can not be seen reliable.

When calculating the bed-to-tube heat transfer coefficient according to the different correlations, there were many assumptions for the properties of the bed material, including emissivity, and sphericity, which was not investigated in this study. As ilmenite is a rather uninvestigated material, the heat capacity together with thermal conductivity is not considered completely accurate. Other possible sources of errors in the experimental part will be discussed in next section.

5.2 Possible sources of error

As it is a experimental investigation, the human factor plays a role in the result, which is important to take in to account. Other than that, a possible source of error for the experiments can be the assumed continuous water flow which was set by a valve and then measured by weighting the collected water during a specific time. It is hard to determine if the flow was constant during the experiments, and also hard to determine exactly with the timing. But experiments was done to prove that small changes in water flow does not affect the heat transfer coefficient significantly.

The amount of the bed material in the reactor was also decided from the bulk density, to get the same bed height for all experiments. The bulk density was only measured for a small sample of the material, thereby it is not true if it represent the whole batch of material as it can differ within the material.

The temperature was only measured at one point close to the tube in the bed, since the bed can be assumed to have a uniform temperature. Despite this, the single measurement point can differ from the rest of the bed, which should be seen as a source of error. When changing between the different fluidization gases, the bed responded by changing temperature. This was probably due to temperature

differences between the gases. The fluidization gases was heated up in the windbox, and depending on the temperature of the gas when it enter the bed it either heat up or cool down the bed, as well as the tube. This may impact the result and the estimated heat transfer for the different fluidization medium.

5.3 Recommendations for future research

Further research within this topic is important in order to determine more accurate heat transfer coefficients by the correlations. This can include more research about properties of ilmenite that are relevant for the heat transfer, for example emissivity, heat capacity, thermal conductivity and sphericity.

As the result with the cases where pure steam was fluidizing the bed has reasons to be considered to be incorrect, it can be of interest to further investigate the influence on the heat transfer by using steam as fluidization gas.

In order to get a more reliable determination of the heat transfer coefficient for the industry, fuel in reactor could be introduced in the reactor to study the difference where the heat comes from the fuel reaction in the reactor compared to when the heat comes from an outside source.

It can also be of interest to study the effect of up-scaling of the reactor, and see if it affects the result. Since it is often the economy that controls the development of new processes, it would also be of interest to study the economical benefits of changing bed material and fluidization gas to increase the heat transfer compared to the cost of these materials to see if it is economical profitable.

6

Conclusion

This study have experimentally investigated the influence of the bed-to-tube heat transfer coefficient by changing the bed material, particle size and fluidization gas at different temperatures. These experimental values were then compared to correlations used for calculating the heat transfer coefficient. The conclusions that can be drawn from this work was:

- Ilmenite showed generally higher heat transfer coefficients compared to sand at the corresponding particle size range, with an average of 2.8 % higher heat transfer coefficient compared to sand.
- Smaller particle size resulted in higher heat transfer coefficient.
- Flue gas influenced the heat transfer coefficient with an average increase of 9.9% compared to air as fluidization medium.
- No single correlation could perfectly describe the heat transfer coefficient, but the correlation by Grewal & Saxena had the highest accuracy for most of the cases.

References

[1] IPCC, "Climate change 2014: Synthesis report", Geneva, Switzerland, 2014.

[2] M. Rydén and A. Lyngfelt, "Using steam reforming to produce hydrogen with carbon dioxide capture by chemical-looping combustion", *International Journal of Hydrogen Energy*, vol. 31, no. 10, pp. 1271–1283, 2006.

[3] A. Lyngfelt, B. Leckner, and T. Mattisson, "A fluidized-bed combustion process with inherent co_2 separation; application of chemical-looping combustion", *Chemical Engineering Science*, vol. 56, no. 10, pp. 3101–3113, 2001.

[4] H. Leion, A. Lyngfelt, M. Johansson, E. Jerndal, and T. Mattisson, "The use of ilmenite as an oxygen carrier in chemical looping combustion", *Chemical Engineering Research and Design*, vol. 86, pp. 1017–1026, 2008.

[5] D. Kunii and O. Levenspiel, *Fluizidation Engineering*. Butterworth-Heinemann, 1991.

[6] V. Stenberg, M. Rydén, T. Mattisson, and A. Lyngfelt, "Exploring novel hydrogen production processes by integration of steam methane reforming with chemical-looping combustion (clc-smr) and oxygen carrier aided combustion (ocac-smr)", *International Journal of Greenhouse Gas Control*, vol. 74, pp. 28–39, 2018.

[7] V. Stenberg, V. Sköldberg, L. Öhrby, and M. Rydén, "Evaluation of bed-to-tube surface heat transfer coefficient for a horizontal tube in bubbling fluidized bed at high temperature", *Powder Technology*, vol. 352, pp. 488–500, 2019.

[8] P. Basu, "Heat transfer", in *Combustion and gasification in fluidized beds*, Boca Raton: CRC Press, 2006.

[9] B. Leckner, "Heat and mass transfer", in *Multiphase Flow Handbook*, E. Michaelides, C. T. Crowe, and J. D. Schwarzkopf, Eds., 2nd, Boca Raton: CRC Press, 2017.

[10] V. Stenberg, F. Lind, and M. Rydén, "Measurement of bed-to-tube surface heat transfer coefficient to a vertically immersed u-tube in bubbling loop seal of a cfb boiler", 2019.

[11] P. O'Kelly, "Heat transfer", in *Computer Simulation of Thermal Plant Operations*, New York: Springer, 2013.

[12] P. Basu, "Hydrodynamics", in *Combustion and gasification in fluidized beds*, Boca Raton: CRC Press, 2006.

[13] ——, "Characteristics of solid particles", in *Combustion and gasification in fluidized beds*, Boca Raton: CRC Press, 2006.

[14] C. Y. Wen and Y. H. Yu, "A generalized method for predicting the minimum fluidization velocity", *A.I.Ch.E. Journal*, no. 12, pp. 610–612, 1966.

[15] Y. Shao, W. Zhong, Z. Bian, and A. Yu, "Minimum fluidization velocity of particles with different size distributions at elevated pressures and temperatures", *Chemical Engineering Science*, 2020.

[16] T. Pröll, "Fundamentals of chemical looping combustion and introduction to clc reactor design", in *Calcium and Chemical Looping Technology for Power Generation and Carbon Dioxide (CO2) Capture*, P. Fennell and B. Anthony, Eds., Woodhead Publishing, 2015.

[17] A. Lyngfelt, "Oxygen carriers for chemical-looping combustion", in *Calcium and Chemical Looping Technology for Power Generation and Carbon Dioxide (CO2) Capture*, P. Fennell and B. Anthony, Eds., Woodhead Publishing, 2015.

[18] M. Rydén, M. Hanning, A. Corcoran, and F. Lind, "Oxygen carrier aided combustion (ocac) of wood chips in a semi-commercial circulating fluidized bed boiler using manganese ore as bed material", *Applied sciences*, vol. 6, no. 11, p. 347, 2016.

[19] MRC. (2020). Mineral sands, Mineral Commodities Ltd., [Online]. Available: `https://www.mineralcommodities.com/products-sales/mineral-sands/` (visited on 02/18/2020).

[20] A. Corcoran, P. Knutsson, F. Lind, and H. Thunman, "Comparing the structural development of sand and rock ilmenite during long-term exposure in a biomass fired 12 mwth cfb-boiler", *Fuel Processing Technology*, vol. 171, pp. 39–44, 2018.

[21] A. Corcoran, "Investigation on ilmenite used for oxygen carrier aided combustion", Chalmers University of Technology, Gothenburg, Sweden, 2017.

[22] J. Adanez, A. Abad, F. Garcia-Labiano, P. Gayan, and L. F. de Diego, "Progress in chemical-looping combustion and reforming technologies", *Progress in Energy and Combustion Science*, vol. 38, pp. 215–282, 2012.

[23] J. R. Welty, G. L. Rorrer, and D. G. Foster, "Fundamentals of heat transfer", in *Fundamentals of Momentum, Heat and Mass Transfer*, 6th ed., Singapore: John Wiley & Sons, 2015.

[24] R. K. Sinnott, J. M. Coulson, and J. F. Richardson, "Heat transfer equipment", in *Chemical Engineering Design*, 4th ed., vol. 6, Elsevier Science & Technology, 2005.

[25] J. H. Lienhard, *A Heat Transfer Textbook*, 5th ed. Courier Dover Publications, 2019, p. 784.

[26] P. C. Bisognin, J. C. S. Câmara Bastos, H. F. Meier, N. Padoin, and C. Soares, "Influence of different parameters on the tube-to-bed heat transfer coefficient in a gas-solid fluidized bed heat exchanger", *Chemical Engineering and Processing: Process Intensification*, vol. 147, 2020.

[27] H. A. Vreedenberg, "Heat transfer between a fluidized bed and a horizontal tube", *Chemical Engineering Science*, vol. 9, pp. 52–60, 1958.

[28] V. A. Ainshtein, "An investigation of heat transfer process between fluidized beds and single tubes submerged in the bed", in *S. S. Zabordsky, "Hydrodynamics and Heat Transfer in Fluidized Beds"*, Cambridge, Massachusetts: M.I.T. Press, 1966, pp. 270–272.

[29] V. G. Ainshtein and N. I. Gelperin, "Heat transfer between a fluidized bed and a surface", *International Chemical Engineering*, vol. 6, no. 1, p. 67, 1966.

[30] W. E. Genetti, R. A. Schmall, and E. S. Grimmett, "The effect of tube orientation on heat transfer with bare and finned tubes in a fluidized bed", *Chemical Engineering Progress Symposium Series*, vol. 67, pp. 90–96, 1971.

[31] B. R. Andeen and L. R. Glicksman, "Heat transfer to horizontal tubes in shallow fluidized beds", *ASME paper*, pp. 9–11, 1976.

[32] N. S. Grewal and S. C. Saxena, "Heat transfer between a horizontal tube and a gas-solid fluidized bed", *Int. J. Heat Mass Transfer*, vol. 23, pp. 1505–1519, 1980.

[33] A. Luckos and P. den Hoed, "Fluidization and flow regimes of titaniferous solids", *Ind. Eng. Chem. Res.*, no. 43, pp. 5645–5652, 2004.

[34] F. P. Incropera, D. P. Dewitt, T. L. Bergman, and A. S. Lavine, *Principles of heat and mass transfer*, 6th ed. John Wiley Sons, 2007.

[35] L. M. Anovitz, A. H. Treiman, E. J. Essene, B. S. Hemingway, E. F. Westrum jr., V. J. Wall, R. Burriel, and S. R. Bohlen, "The heat-capacity of ilmenite and phase equilibria in the system fe-ti-o*", *Geochimica et Cosmochimica Acta*, vol. 49, pp. 2027–2040, 1985.

A

Appendix 1

A.1 jh correlation

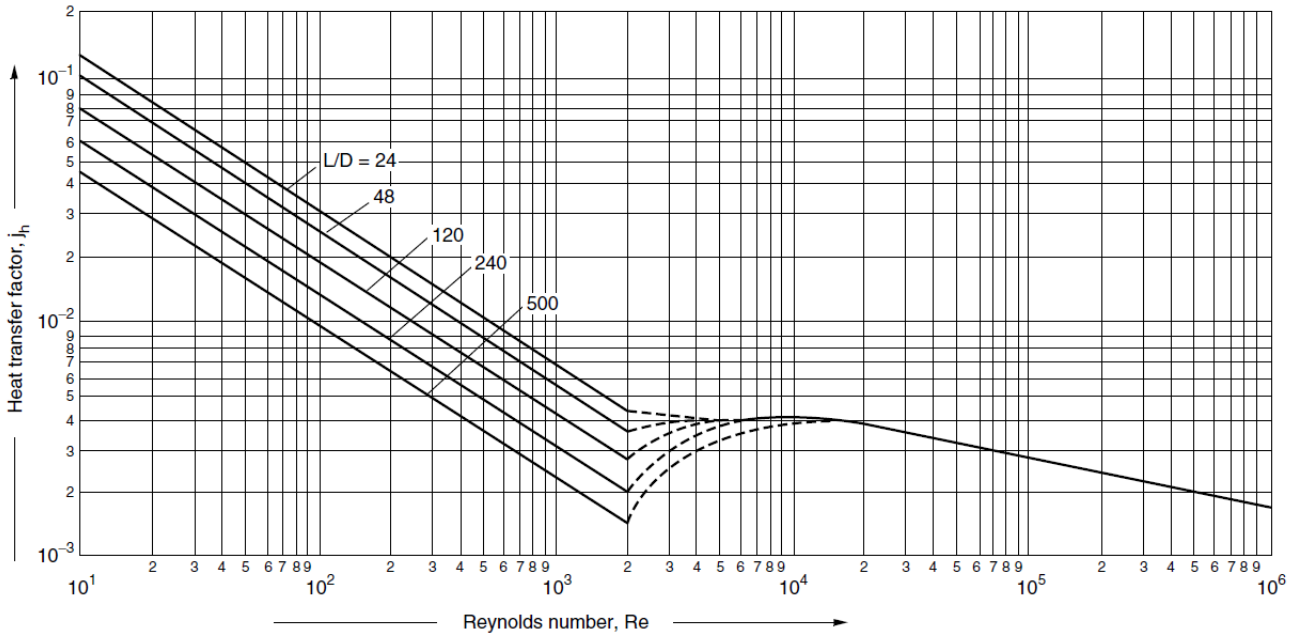

Figure A.1: Tube side heat transfer factor

A.2 Correlations comparison

A.2.1 Ilmenite 90-150μm

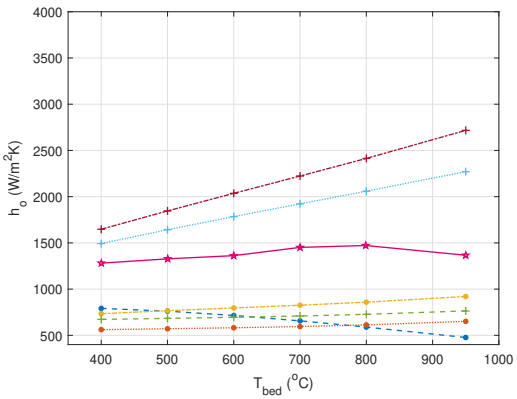

(a) Case 1. Fluidization medium: Air.

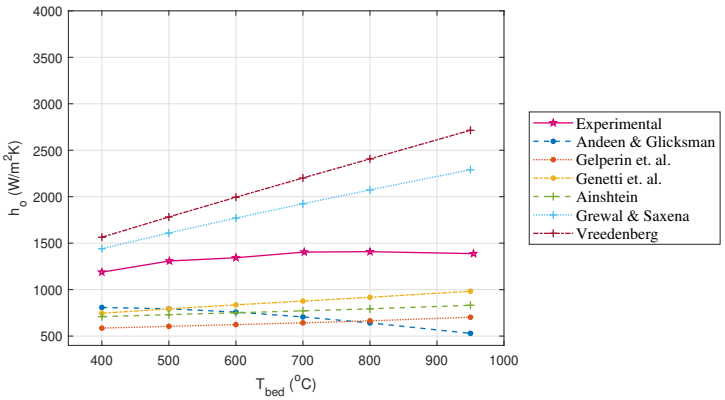

(b) Case 2. Fluidization medium: CO_2.

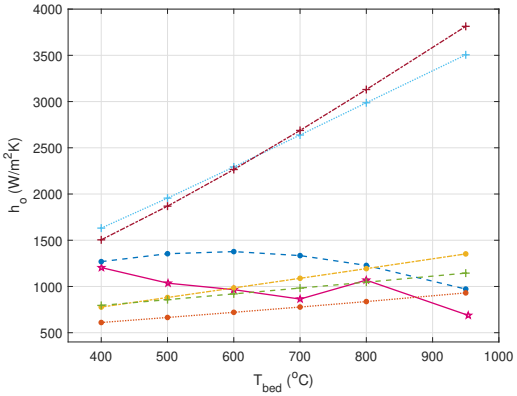

(c) Case 3. Fluidization medium: Steam.

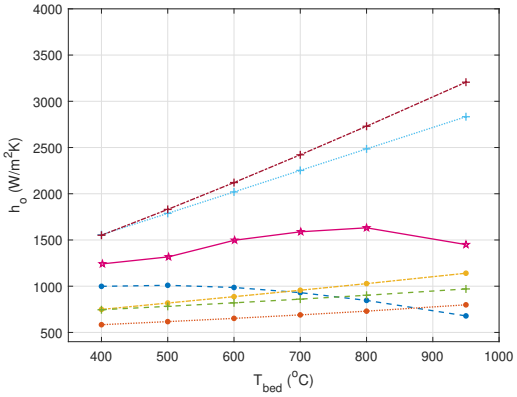

(d) Case 4. Fluidization medium: Flue gas.

Figure A.2: Case 1-4 using Ilmenite 90-150 μm as bed material.

A.2.2 Ilmenite 150-212 μm

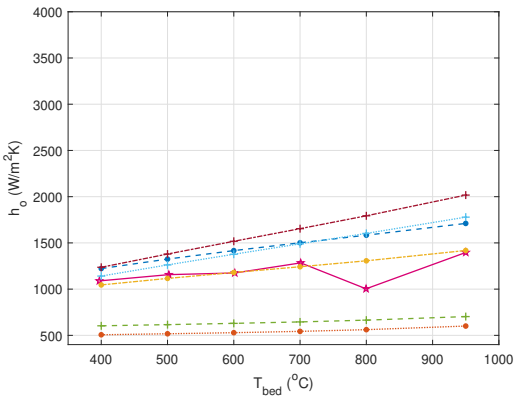

(a) Case 5. Fluidization medium: Air.

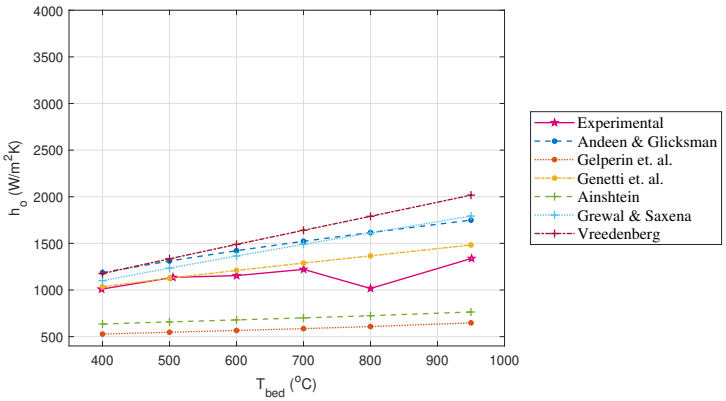

(b) Case 6. Fluidization medium: CO_2.

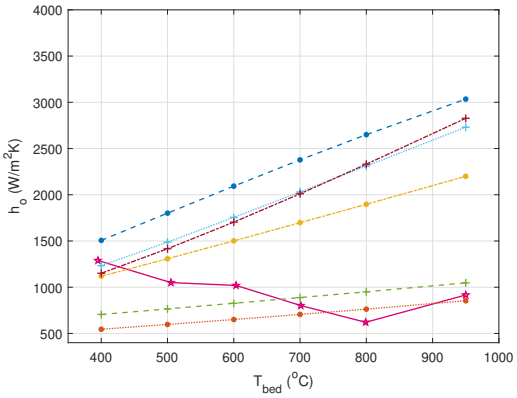

(c) Case 7. Fluidization medium: Steam.

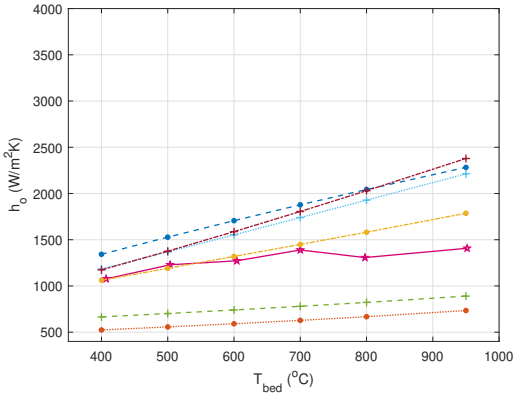

(d) Case 8. Fluidization medium: Flue gas.

Figure A.3: Case 5-8 using Ilmenite 150-212 μm as bed material.

Ilmenite 212-250 μm

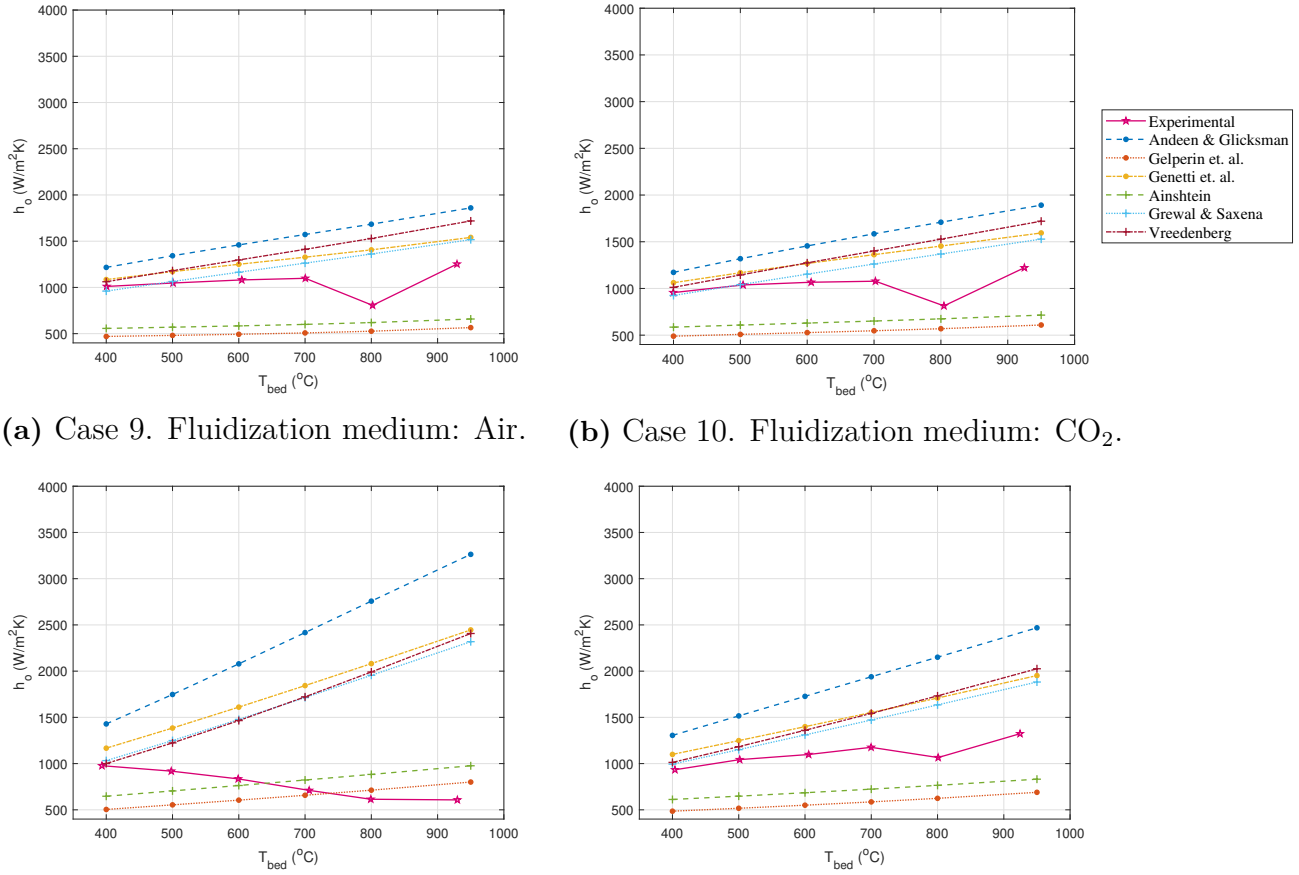

(a) Case 9. Fluidization medium: Air.

(b) Case 10. Fluidization medium: CO_2.

(c) Case 11. Fluidization medium: Steam.

(d) Case 12. Fluidization medium: Flue gas.

Figure A.4: Case 9-12 using Ilmenite 212-250 μm as bed material.

A.2.3 Ilmenite 250-355 μm

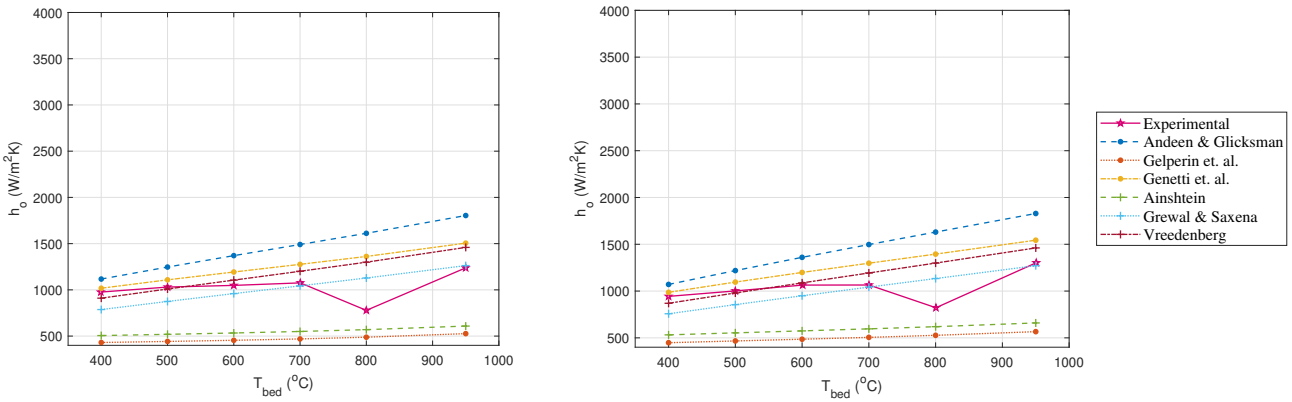

(a) Case 13. Fluidization medium: Air.

(b) Case 14. Fluidization medium: CO_2.

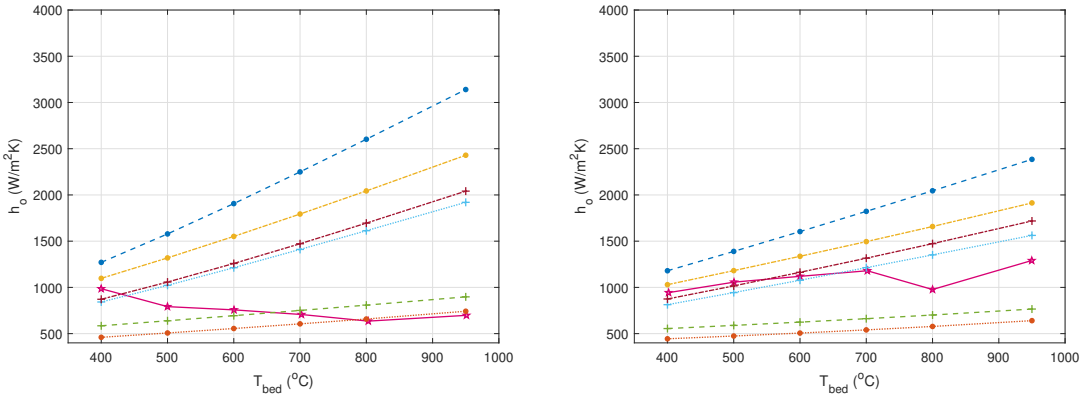

(c) Case 15. Fluidization medium: Steam.

(d) Case 16. Fluidization medium: Flue gas.

Figure A.5: Case 13-16 using Ilmenite 250-355 μm as bed material.

A.2.4 Sand 90-150μm

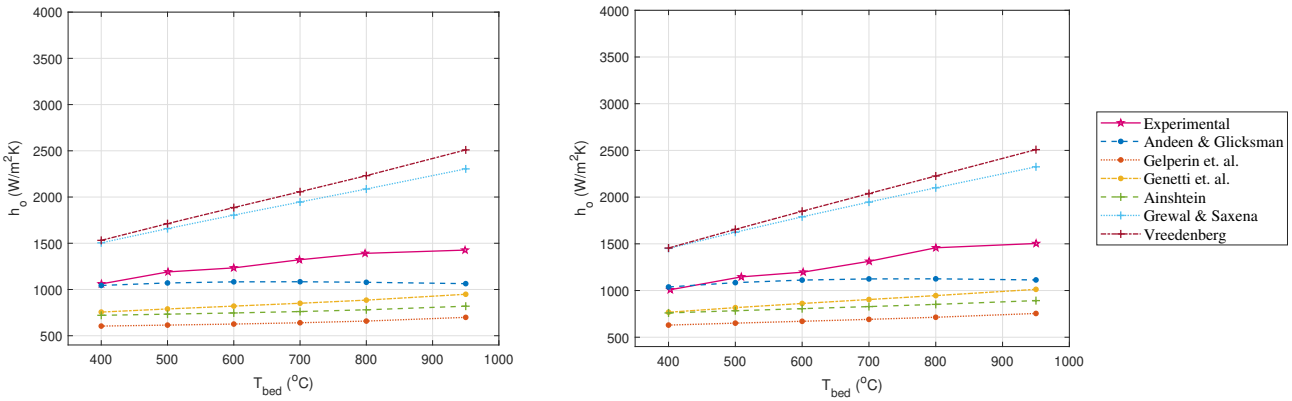

(a) Case 17. Fluidization medium: Air.

(b) Case 18. Fluidization medium: CO_2.

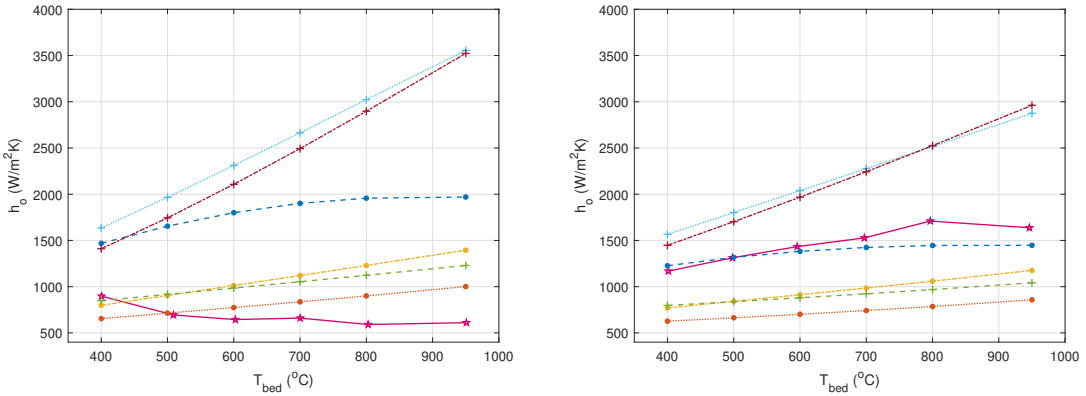

(c) Case 19. Fluidization medium: Steam.

(d) Case 20. Fluidization medium: Flue gas.

Figure A.6: Case 17-20 using Sand 90-150 μm as bed material.

A.2.5 Sand 150-212 μm

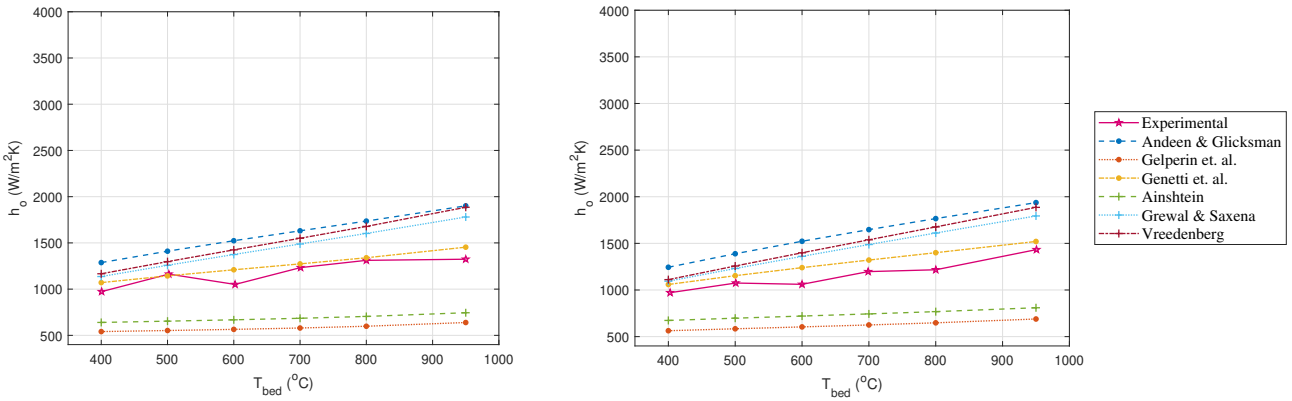

(a) Case 21. Fluidization medium: Air.

(b) Case 22. Fluidization medium: CO_2.

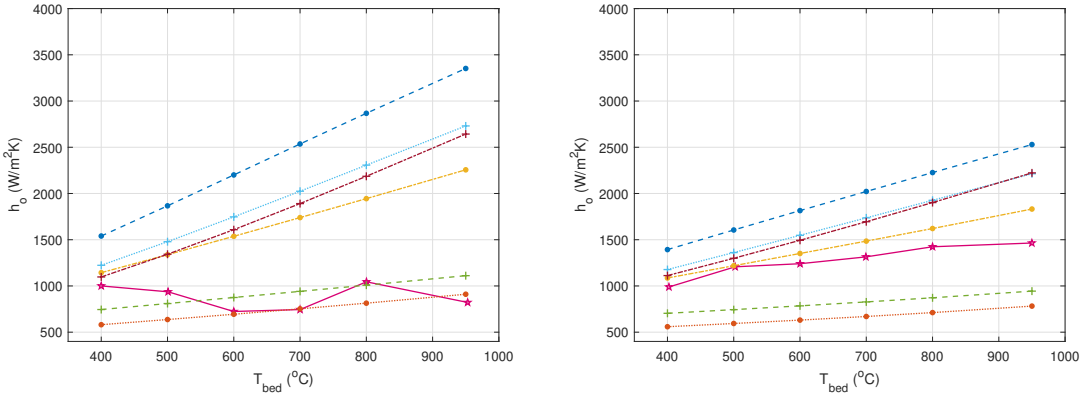

(c) Case 23. Fluidization medium: Steam.

(d) Case 24. Fluidization medium: Flue gas.

Figure A.7: Case 21-24 using Sand 150-212 μm as bed material.

A.2.6 Sand 212-250 μm

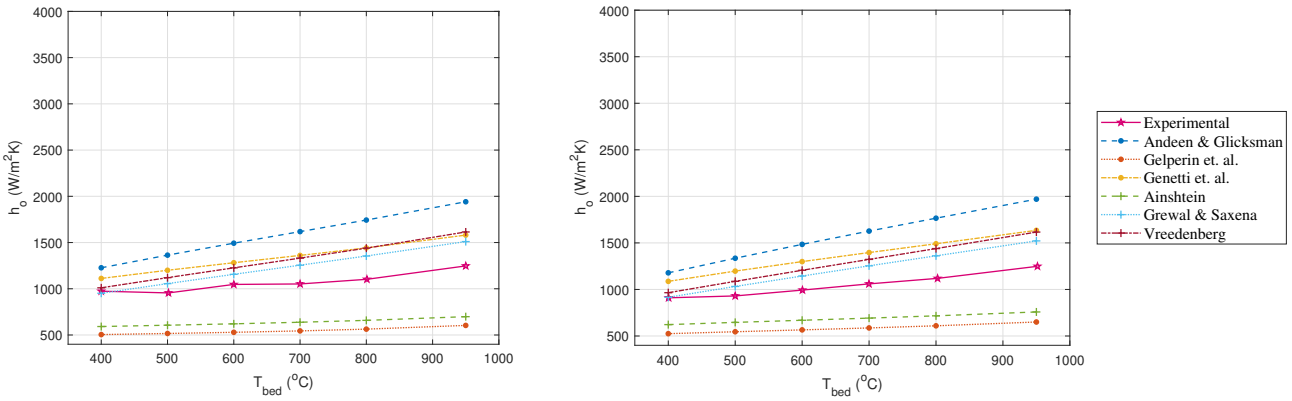

(a) Case 25. Fluidization medium: Air.

(b) Case 26. Fluidization medium: CO_2.

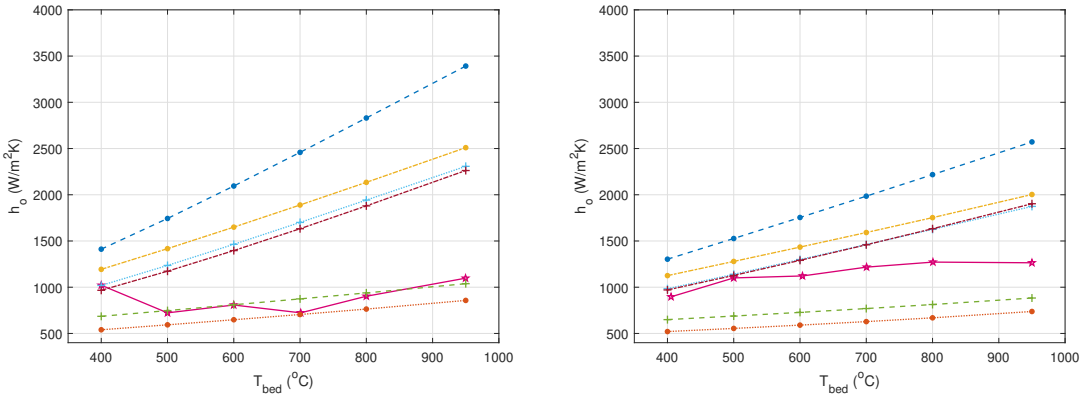

(c) Case 27. Fluidization medium: Steam.

(d) Case 28. Fluidization medium: Flue gas.

Figure A.8: Case 25-28 using Sand 212-250 μm as bed material.

A.2.7 Sand 250-355 μm

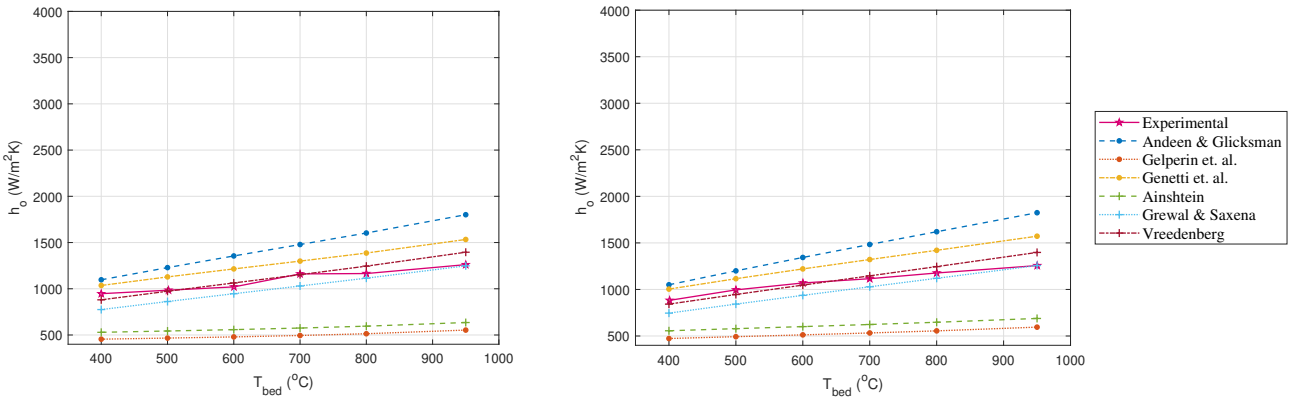

(a) Case 29. Fluidization medium: Air.

(b) Case 30. Fluidization medium: CO_2.

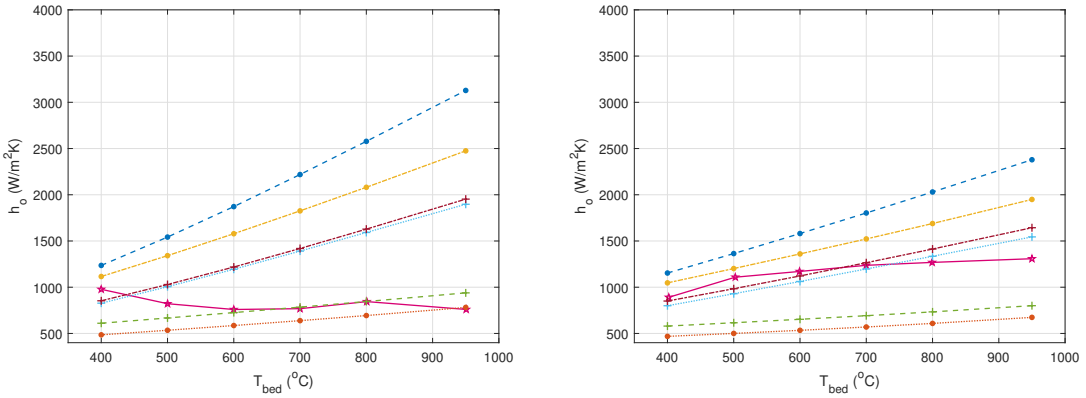

(c) Case 31. Fluidization medium: Steam.

(d) Case 32. Fluidization medium: Flue gas.

Figure A.9: Case 29-32 using Sand 250-355 μm as bed material.